AGU ADVANCING EARTH AND SPACE SCIENCES

Earth and Space Science

RESEARCH ARTICLE
10.1029/2024EA003563

Changing Extreme Precipitation Patterns in Nepal Over 1971–2015

Yinxue Luo[1], Lang Wang[2], Chenxi Hu[3,4], Lu Hao[1], and Ge Sun[5]

[1]Collaborative Innovation Center on Forecast and Evaluation of Meteorological Disasters (CIC-FEMD)/Key Laboratory of Ecosystem Carbon Source and Sink, China Meteorological Administration (ECSS-CMA), Nanjing University of Information Science and Technology, Nanjing, China, [2]Department of Geography and Resource Management, The Chinese University of Hong Kong, Hong Kong, China, [3]Earth and Environmental Sciences Programme, The Chinese University of Hong Kong, Hong Kong, China, [4]Department of Earth and Planetary Sciences, Jackson School of Geosciences, The University of Texas at Austin, Austin, TX, USA, [5]Eastern Forest Environmental Threat Assessment Center, Southern Research Station, USDA Forest Service, Research Triangle Park, NC, USA

Key Points:

- From 1971 to 2015, extreme precipitation events decreased in Nepal overall, with the west getting wetter and the east drier post-2003
- The APHRODITE gridded reliably reproduces Nepal's extreme precipitation
- Changes in precipitation are the results of variations in monsoon intensity and shifts in wind patterns

Supporting Information:

Supporting Information may be found in the online version of this article.

Correspondence to:

L. Wang,
lang.wang.mq@gmail.com

Citation:

Luo, Y., Wang, L., Hu, C., Hao, L., & Sun, G. (2024). Changing extreme precipitation patterns in Nepal over 1971–2015. *Earth and Space Science*, *11*, e2024EA003563. https://doi.org/10.1029/2024EA003563

Received 30 JAN 2024
Accepted 7 OCT 2024

Author Contributions:

Conceptualization: Yinxue Luo, Lang Wang, Chenxi Hu, Lu Hao, Ge Sun
Data curation: Lang Wang
Formal analysis: Lang Wang
Investigation: Lang Wang
Methodology: Lang Wang
Resources: Lang Wang
Software: Yinxue Luo
Supervision: Lang Wang, Chenxi Hu, Lu Hao, Ge Sun
Validation: Lang Wang
Visualization: Yinxue Luo
Writing – original draft: Yinxue Luo, Lang Wang, Chenxi Hu
Writing – review & editing: Lang Wang, Chenxi Hu, Lu Hao, Ge Sun

Abstract This paper provides a comprehensive and comparative analysis of extreme precipitation patterns from 1971 to 2015 in Nepal, a data scarce, but "hot spot" region in global climate change. We compare in-situ observations and gridded precipitation data from the Asian Precipitation Highly Resolved Observational Data Integration Toward Evaluation of Water Resources (APHRODITE). Using 11 precipitation indices, we show that high-intensity (RX1day, R95pTOT, R99pTOT) and frequency-related indices (R10 mm, R20 mm) have decreased but annual maximum consecutive dry and wet days have increased. Observations affirm these trends found by the APHRODITE, but show smaller magnitudes likely due to differences in measurements at locations made below the 3,000 m elevation line. Spatially, the relatively dry western region has become wetter, and the relatively wet eastern region has become drier post-2003. The weakening of the South Asia Monsoon circulation, particularly assessed by the Webster and Yang Monsoon Index, correlates strongly with extreme precipitation indices. Changes in upper-level jet and associated lower-level monsoon trough are identified as critical factors influencing the extreme precipitation trend post-2003. This study is the first to confirm the efficacy of APHRODITE in providing spatial and temporal precipitation patterns in a data-limited region. We conclude that monsoon weakened circulations and changes in regional wind fields play dominant roles in the long-term temporal and spatial trends of extreme precipitation in Nepal. The reduced precipitation extremes in the wet eastern region may somewhat lessen severe flooding and erosion, but the drier western region may face heightened risks in precipitation-related hazards in Nepal.

Plain Language Summary Precipitation is one of the most important components of the Earth's water cycles but is least predictable locally amid global climate change. Understanding the historical dynamics of extreme precipitation provides critical information for developing climate mitigation and adaptation strategies. This paper examines extreme precipitation patterns in Nepal from 1971 to 2015. Comparing observations on site and Asian Precipitation Highly Resolved Observational Data Integration data, the study identifies decreasing intense and frequent rainfall and increasing prolonged precipitation. On-site data show similar trends to the integration data, but have smaller magnitudes. Post-2003, the west and the east tend to get wetter and drier, respectively. The study links these changes to a weakened South Asia Monsoon circulation, particularly indicated by the Webster and Yang Monsoon Index. The shift in upper-level jet and lower-level monsoon trough are identified as key factors influencing extreme precipitation trends post-2003. This study validates APHRODITE in data-limited regions. The findings suggest that weakened monsoon circulations and changes in wind patterns significantly contribute to long-term trends in extreme precipitation in Nepal. While reduced extremes in the wet eastern region may imply decreased flooding risks, but the drier western region may face increased hazards and ecosystem changes related to precipitation.

1. Introduction

Precipitation, the most vital element of the Earth's water cycle, is undergoing dynamic shifts influenced by global warming and land use change (Sun et al., 2024). The most recent Intergovernmental Panel on Climate Change's Sixth Assessment Report (AR6) warns of a significant increase in global mean surface precipitation since 1950 and a rise in extreme precipitation intensity and occurrences (Seneviratne et al., 2021). These trends have far-

10.1029/2024EA003563

reaching economic and ecological sequences including climate calamities like landslides, floods, and droughts (Donat et al., 2016; Easterling et al., 2000; Fischer & Knutti, 2015; Kotz et al., 2022; Mukherjee et al., 2018; Sun & Ao, 2013; Tabari, 2020). A comprehensive understanding of these evolving precipitation patterns is critical for assessing risks in relation to climate change mitigation and adaptation at a regional scales.

The South Asian Monsoon rains provide up to 80% of the region's total precipitation (Turner & Annamalai, 2012) and has significant implications for regional water resources by industry, agriculture, forestry (Gao et al., 2023), and overall people's well-being (Meehl et al., 2023). Existing evidence indicates a weakening trend in South Asian summer monsoon circulation since the 1950s (Annamalai et al., 2013; Bollasina et al., 2011; Fang et al., 2023; Ramanathan et al., 2005; Roxy et al., 2015). This overall weakening trend has resulted in reduced precipitation overall in South Asia (Kulkarni, 2012; Mishra et al., 2012; Roxy et al., 2015; Turner & Annamalai, 2012; Wang & Ding, 2006). However, a recent recovery since 2000 in monsoon circulation and associated precipitation in northern India has been reported (Jin & Wang, 2017).

Most literature agrees that the decline in monsoon circulation and rainfall variability has amplified in recent decades (Ghosh et al., 2016; Mohan & Rajeevan, 2017; Singh et al., 2014; Vinnarasi & Dhanya, 2016). For example, extreme rainfall events have increased over the Indian subcontinent due to changes in monsoon circulations (Ghosh et al., 2016; Goswami et al., 2006; Krishnan et al., 2016; Roxy et al., 2017; Singh et al., 2014, 2019). Roxy et al. (2017) reported a threefold increase in widespread extreme rain events in central-India. These unprecedented extreme rainfall events and the resulting natural disasters make the densely populated South Asian subcontinent highly vulnerable. The average intensity and frequency of extreme events in the region are growing, and spatial precipitation distributions are increasingly variable (Aggarwal et al., 2022; Ghosh et al., 2016; Krishnan et al., 2016). Thus, it is important to consider the temporal and spatial variability when analyzing extreme precipitation trends in South Asia, where localized variations and topography are important.

Nepal, situated on the north fringes of the South Asian Monsoon region and characterized by large spatial elevation variations, has been the focus of numerous hydroclimatic studies (Bohlinger & Sorteberg, 2018; Karki et al., 2017; Maharjan et al., 2023; Panthi et al., 2015; Pokharel et al., 2020; Shrestha et al., 2019; Talchabhadel et al., 2018; Tuladhar et al., 2020). However, compared to other South Asian countries, research on extreme precipitation and annual precipitation in Nepal has been sporadic and often short in study periods and limited in space. Current understanding is rather fragmented and sometimes inconsistent outcomes. For example, Duncan et al. (2013) using APHRODITE identified widespread decreasing trends across Nepal of extreme events during 1951–2007, with some increases over the Terai regions. However, Baidya et al. (2008) found a rising trend in extreme precipitation intensity and frequency across most meteorological stations in Nepal during a similar period 1961–2006. Two more recent studies found a significant increase in extreme precipitation in the far-western region, and a decrease in the central and eastern mountains in Nepal from the 1970–2010s based on station data (Bohlinger & Sorteberg, 2018; Karki et al., 2017). Yet other study based on station data concluded that extreme precipitation was increasing in the Eastern High Mountains from 1976 to 2015 (Maharjan et al., 2023). These disparate findings can be attributed to the use of different climate data sets, variable study time periods, and distinct study focus, highlighting the need for a comprehensive nationwide perspective.

Another critical research gap on extreme precipitation in Nepal is the lack of process-based understanding of the observed spatial and temporal trends. Extreme rainfall events are influenced by a variety of synoptic-scale features, such as local convective instability, large-scale monsoon activity, anomalous extratropical circulations and their interactions with the monsoon circulation through the Himalayas, and show substantial regional variability (Guhathakurta et al., 2011; Vellore et al., 2014, 2016). Furthermore, globally, the observed rise in precipitation extremes aligns closely with the Clausius–Clapeyron (C-C) rate, an approximate 7% increase for every 1°C warming of in global average surface temperature (Allan et al., 2022; Fischer & Knutti, 2015; Sun & Ao, 2013; Sun et al., 2021; Tabari, 2020). Climate model projections reinforce this trend, highlighting that more moisture leads to a substantial rise in precipitation extremes (RX1day), ranging from 3% to 8% every 1°C of surface warming with high confidence (Pfahl & Wernli, 2012; Seneviratne et al., 2021; Wei et al., 2024). Despite this principle consistency, the increases in precipitation extremes exhibit significant spatial variability (Byrne & O'Gorman, 2018; Saha & Sateesh, 2022), and the influence of thermodynamics-related water vapor factors versus dynamic factors such as potential changes in the strengths of atmospheric circulations varies markedly across regions (Nie et al., 2018). Given mountainous terrain in Nepal and the large influence of the South Asian monsoon climate on the region, patterns of extreme precipitation in Nepal are expected to be complex, and a mechanistic understanding is needed.

According to global projections, extreme precipitation in most parts of the subcontinent will be further exacerbated by the end of this century. There is an immediate need to understand these extremes. Therefore, this study seeks to give answers to the questions:

(a) Is the APHRODITE data set consistent with station-based local data in Nepal's geographically diverse regions? (b) Are there discernible long-term trends and patterns in extreme precipitation in Nepal confronting a changing climate? and (c) What are the factors that predominantly influence the long-term trends and patterns in extreme precipitation changes in Nepal?

This study aims to address these three questions and provide a comprehensive assessment of changes in the intensity, occurrence, and duration of extreme precipitation events in Nepal. We utilized the APHRODITE and DHM data sets and employed metrics, including the Pearson correlation coefficient, to investigate correlations between the data sets. Additionally, trend analyses were conducted using the Mann-Kendall trend test in conjunction with the Sen's slope estimator, and the Pettitt turning-point detection method. The study also examined the dominant factors that directly contribute to changes in extreme precipitation in Nepal.

2. Methods and Data Sets

2.1. Study Area

Nepal lies between 26°22′N and 30°27′N in latitude, and 80°04′E to 88°12′E in longitude on the southern slope of the Himalayas (Figure 1a). Nepal's predominantly mountainous terrain exhibits a distinctive elevation range, from 60 m to over 8,000 m in a short distance. The nation can be classified into five geographic sectors: the Terai, the Siwaliks, the Middle Mountains, the High Mountains, and the High Himalaya. The Terai has altitudes ranging from 60 to 300 m, representing the northern extension of the Indo-Gangetic Plain and about 13% of Nepal's total land area. The Siwaliks represents the foothill belt that accounts for about 12% of the total area with an elevation less than 1,000 m. The Middle Mountains cover about 30% of the total area, with the elevation from 1,000 to 2,000 m. This zone is the first effectual barrier to the monsoon clouds entering the Himalayas and has a considerable impact on the country's rainfall pattern. The High Mountains cover about 20% of the total area with altitudes ranging from 2000 to 4,000 m. The High Himalayas in the north occupy nearly 24% of the total area at an altitude of over 4,000 m. This topographical variability results in a wide range of climate types, spanning from tropical savannah to polar climates. Nepal experiences four distinct seasons directly associated with the monsoon cycle: pre-monsoon (March–May), summer monsoon (June–September), post-monsoon (October–November), and winter (December–February). Most of the precipitation (∼80%) occurs during the summer monsoon season (Sharma et al., 2020) (Figures 1b–1e). Precipitation in Nepal is governed by two main climate systems. During the monsoon season, the South Asian monsoon has a strong influence on the southeastern part of the country; and during the winter season, the western disturbances mainly affect the northwestern alpine regions. Precipitation patterns are largely determined by the geomorphic effects of the complex topography of the central Himalayas and the east-west shift of the summer monsoon. As a result, Nepal's precipitation has great variability in its spatial distribution (Figures 1b–1e). The wetter areas are mostly on the windward side of the South Asian monsoon, with the greatest amount of precipitation occurring along the ridges from east to west. The leeward side of the alpine regions receives less precipitation. Both the APHRODITE gridded data set (Yatagai et al., 2012) and station-based observations precipitation data sets (1971–2015) point to two significant parallel precipitation peak areas: the first at about 1 km above mean sea level and the second at about 2 km above sea level. In some high mountain areas, precipitation peaks at approximately 2,500–3,600 mm and then falls off with rising altitude.

2.2. Data Sets

2.2.1. Station-Based Meteorology Data

The daily stational precipitation data from 1971 to 2015 were acquired from the Department of Hydrology and Meteorology (DHM) of Nepal. To assure an even spatial distribution of weather stations and to capitalize on as many high-quality sequential observations as possible, we limited the study period to 1971–2015. For quality control, the station data set was further filtered to meet the conditions: (a) missing daily observation days should be less than or equal to 15 days in a year, and missing days in a given month cannot exceed 3 days; (b) months with

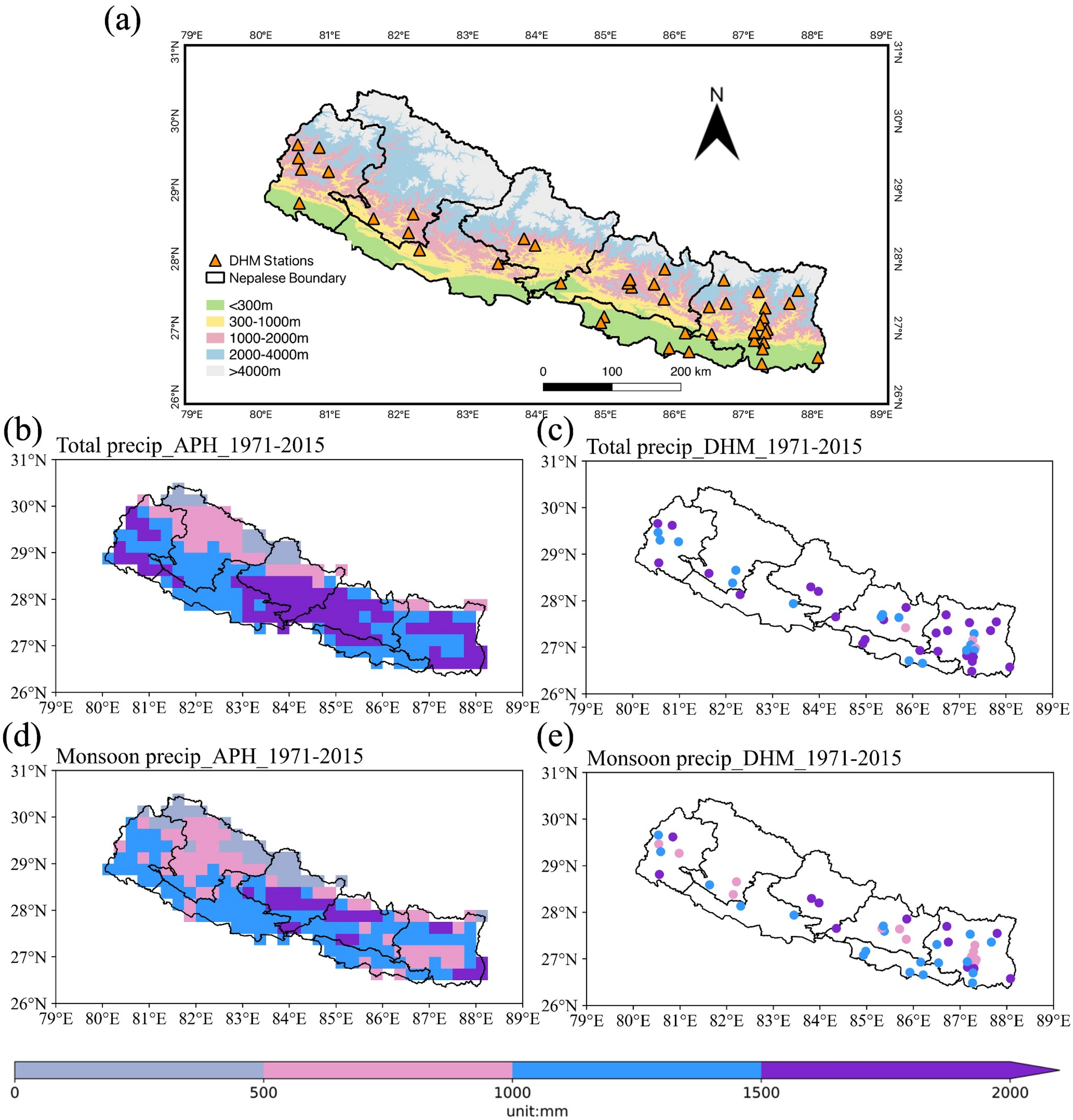

Figure 1. Topography and precipitation patterns in Nepal: (a). Topography (shaded) and station locations (triangles) utilized in this study (refer to Table S1 in Supporting Information S1 for a comprehensive list of stations), (b, c) annual precipitation climatology from 1971 to 2015 using the APHRODITE gridded data set (abbreviated as APH) and the Department of Hydrology and Meteorology (DHM) in-situ data set (abbreviated as DHM), respectively, and (d, e) monsoon precipitation climatology using the two data sets, respectively.

more than 3 days of missing observations are set as missing; (c) a year with more than 15 days of missing observations is set as missing. Additionally, for long-term records, the number of years with missing records is less than 15% of the total years of the study period. Forty-four stations were selected in this study. Using these stations, an extended period of 2016–2020 is also considered to detect any further changes. Consequently, 68.2% of the stations are located in areas with longitudes greater than the central line 84.5°E (Figure 1a). However, all stations

10.1029/2024EA003563

are located below the 3,000 m elevation threshold as maintaining weather stations in high-altitude areas is challenging (Table S1 in Supporting Information S1). We chose 83 stations for validation purposes from the period 1981–2015, aligning with the overlapping timeframe of the other gridded precipitation data sets (Table S1 in Supporting Information S1).

2.2.2. APHRODITE and Other Gridded Precipitation Data

In addition to station-based climate data, we also examined the published APHRODITE gridded precipitation data to better understand the full spatial and temporal distributions of precipitation. APHRODITE is a long term (1951 onwards) set of continental scale daily products built on a densely distributed network of rain gauge data in Asia (Yatagai et al., 2012). The dense network of rain-gauge data for Asia including the Himalayas. The high density of input stations, interpolation scheme, and quality control of data allow for the study of detailed extreme events. It is considered to be one of the best gridded precipitation products in Asia (Ménégoz et al., 2013). Daily-scale precipitation data from version APHRO_MA_V1101 (1971–2007) as well as version APHRO_MA_-V1101_extra (2008–2015), which cover the South Asian monsoon region with a spatial resolution of 0.25°, were used to calculate the long-duration precipitation series from 1971 to 2015. The agreement with station observed DHM data were assessed in the study over Nepal (Figures S1–S7, Tables S2–S3 in Supporting Information S1).

We also assessed other existing precipitation data sets that have the potential to provide improved extreme precipitation indices in Nepal. The data sets included the Third Pole High-resolution Precipitation data set (TPHiPr) (H. Jiang, Yi, et al., 2023). It is currently the highest resolution (1/30°, 1d) and highest time-series completeness gridded product in the Third Pole region and is believed to be good at detecting precipitation changes in the Third Pole region (Y. Jiang, Yi, et al., 2023).

The Climate Hazards Group InfraRed Precipitation with Station (CHIRPS) (Funk et al., 2015), a satellite-based observation data integration product, has become a widely used precipitation product in recent years due to its long time-series and high continuity. In fact, CHIRPS is widely used as input data to hydrological models which are mostly at basin scale. And CHIRPS has performed well in reproducing regional precipitation in Nepal and India, especially monsoon precipitation (Aryal et al., 2023; Dangol et al., 2022; Gupta et al., 2020; Khatakho et al., 2021; N. K. Shrestha, Qamer, et al., 2017; Talchabhadel et al., 2021; Upadhyay et al., 2022; Yigez et al., 2022). The data set has a potential for extreme precipitation study at the national scale.

The ERA5-land precipitation data from the European Center for Medium-Range Weather Forecasts (ECMWF) is the reanalysis model precipitation data that is widely used in precipitation studies (Service, 2019). The ERA5-land precipitation data set has a bias of less than 15% in tracking large storm events in the eastern Himalaya and has been recommended for use in studies to understand extreme events and geo-hazards in the region (Kumar et al., 2021).

Both temporal and spatial patterns of extreme precipitation indices were compared to assess overall agreements (Figures S1–S4 in Supporting Information S1). We found that APHRODITE performed the best amongst the data sets in agreeing with DHM station data during the overlapped period. Therefore, APHRODITE was chosen for further analysis. Analyses with other four data sets were not presented with results listed in Supplementary instead (Figures S1 and S2 in Supporting Information S1).

2.2.3. ERA5 Reanalysis Data

The reanalysis data set of the European Center for Medium-Range Weather Forecasts (ECMWF) Reanalysis v5 (ERA5) was adopted for the study to learn the mechanisms behind the extreme precipitation patterns over Nepal. We utilized the u and v components of wind across vertical levels over Nepal from 1971 to 2015 at a resolution of $0.25° \times 0.25°$ on a daily basis (Hersbach et al., 2023b). The atmospheric pressure levels of 850 hPa, 500 hPa, 200 hPa and the vertical integral of water vapor flux were considered in the study to characterize wind conditions for low, medium, and upper level and water vapor budget (Hersbach et al., 2023a).

2.2.4. India Dipole Mode (IOD) Index

The IOD index is defined as the difference between the mean sea surface temperature (SST) in the tropical western Indian Ocean (50°–70°E, 10S°–10°N) and the equatorial southeastern Indian Ocean (90°–110°E, 10°S–0°N). During the positive phase, warm water is pushed to the western Indian Ocean, while cold water is located at the eastern Indian Ocean. During negative phase, this pattern is reversed. The east-west SST contrast in Indian Ocean could significantly affect the strength of the circulation via altering lower level wind field and moisture from the ocean. Data of IOD index were from the National Aeronautics and Space Administration (NOAA) of the United States, including annual and monsoon (June–September) values (Saji et al., 1999).

2.3. Monsoon Circulation Index

Apart from the upper-level atmospheric variables, three monsoon circulation indices were adopted for characterizing large-scale monsoonal circulations. Regional level monsoon indices include Webster and Yang Index (WYI), the Indian Monsoon Index (IMI), and South Asian Summer Monsoon Index (SASMI). WYI is defined as the difference between the high- and low-level latitudinal winds in the Asian monsoon region (Webster & Yang, 1992). It can well interpret the north-south thermal contrast. The higher WYI represents stronger vertical wind shear, which means stronger monsoon circulation, and vice versa. The advantage of WYI is that it is simple to calculate, has a clear physical meaning, and is suitable for describing the changes of the monsoon circulation on a large scale.

The IMI is a shear vorticity index It not only reflects well the average rainfall anomalies over a wide area including the Bay of Bengal, India and the eastern Arabian Sea, but is also highly correlated with the all-India summer rainfall and could potentially be used for Nepal rainfall analysis (Wang & Fan, 1999).

SASMI is also an index that describes the monsoon changes in South Asia. It is based on the seasonality of wind field. SASMI is defined as the area-averaged dynamically normalized seasonality within different domains of South Asia. The significant positive correlation of this index with the summer precipitation field is located in the central and northern parts of India (adjacent to Nepal) and in the Bay of Bengal region (Li & Zeng, 2002). SASMI also measures a broad-scale South Asian Summer Monsoon rather than the regional features.

2.4. Analytical Methods

2.4.1. Trend Detection and Change Point Detection

The Mann-Kendall (MK) Trend Test is used to analyze time series data for consistently increasing or decreasing trends (monotonic trends) (Mann, 1945). The MK test is a non-parametric test and has been widely used in the trend detection of the hydrometeorological time series. The test is based on assumption that observations or data obtained over time are independent and identically distributed. The independence means that the observations are not serially correlated over time.

The Mann kendall test statistic S is calculated as:

$$S = \sum_{\mathrm{i}=1}^{n-1} \sum\nolimits_{j=i+1}^{n} \mathrm{sgn}(x_j - x_i) \tag{1}$$

$$\mathrm{sgn}(x_j - x_i) = \begin{cases} 1, x_j - x_i > 0 \\ 0, x_j - x_i = 0 \\ -1, x_j - x_i < 0 \end{cases} \tag{2}$$

When $n > 10$, the test statistic S is approximately normally distributed with mean equal to zero, and the variance of S is given by:

$$\mathrm{Var}(S) = \frac{1}{18}\left[n(n-1)(2n+5) - \sum_{i=1}^{n} t_i(i)(i-1)(2i+5)\right] \tag{3}$$

where t_i denotes the number of ties in the i range. When $n > 10$, the standard normal variable z is calculated as follows:

$$z = \begin{cases} \frac{S-1}{\sqrt{\mathrm{Var}(S)}}, S > 0 \\ 0, S = 0 \\ \frac{S+1}{\sqrt{\mathrm{Var}(S)}}, S < 0 \end{cases} \tag{4}$$

In a two-tailed test for trend, the null hypothesis is rejected if $|z| > \frac{z_\alpha}{2}$.

However, observations in hydrometeorological time series are often autocorrelated. This makes it important to check the autocorrelation in a given series and to adjust the test if necessary (Hamed & Rao, 1998; Yue & Wang, 2002). The modified MK test is one approach to eliminate the precipitation data that may has non-stationarity or serial correlation. A variance correction approach for the MK test (Hamed & Rao, 1998) is one of the classic methods for modified MK test to reduce the error caused by serial correlation. This modified MK method has been validated to have a greater power to reflect the true significance of trends in precipitation and streamflow series (Hamed & Rao, 1998).

The modified MK test using corrected variance is calculated using the effective sample size to compensate for the effect of serial correlation on the variance, and is calculated using the formula:

$$V^*(S) = \mathrm{Var}(S) \times \frac{n}{n_s^*} = 1 + \frac{2}{n(n-1)(n-2)} \times \sum_{i=1}^{n-1} (n-i)(n-i-1)(n-i-2)\rho_s(i) \tag{5}$$

where $\frac{n}{n_s^*}$ denotes the correction to Var(S) due to autocorrelation in the data.

The $\rho_s(i)$ is the autocorrelation function of the data rank. $\rho_s(i)$ is expressed as:

$$\rho_s(i) = \frac{\sum_{i=1}^{N-j} \left[\left(x_i - \overline{\mathrm{X}}\right)\left(x_{i+j} - \overline{\mathrm{X}}\right) \right]}{\sum_{i=1}^{\mathrm{N}} \left(x_i - \overline{\mathrm{X}}\right)^2} \tag{6}$$

where N is the rank number of observations.

Since the MK test only indicates the direction of the trend, the magnitude of the trend is detected using Theil-Sen slope estimation method (Sen et al., 1968). If there is a linear trend in the time series, then the true slope can be determined by a simple non-parametric procedure. The Sen's slope for a monotonically increasing or decreasing time (t) series $f(t)$ is given by:

$$f(t) = Qt + B \tag{7}$$

where Q is the slope of the trend $f(t)$ and B is the intercept.

The following formula can be used to calculate the slope between each data pair:

$$Q_i = \left[\frac{(X_j - X_k)}{(j-k)} \right] \text{where } j > k \tag{8}$$

if there are n X_j values in the time series, then there are $N = \frac{n(n-1)}{2}$ slope estimates of Q_i. The Sen's slope estimator is the median of these N values of Q_i.

The above calculations can be performed directly for temporal series. For spatial data, we looped through latitude and longitude to each of the grids or stations, and then performed the trend test and slope calculation for the series at the particular grid or station.

Table 1
A Description of Extreme Precipitation Indices

Index examined	Abbreviations	Unit	Relevance
Max 1-day precipitation amount	RX1day	mm	High Intensity related (HIR)
Max 5-day precipitation amount	RX5day	mm	
Very wet days (total precipitation of days in >95th percentile)	R95pTOT	mm	
Extremely wet days (total precipitation of days in >99th percentile)	R99pTOT	mm	
Number of heavy precipitation days (count of days when precipitation is ≥10 mm)	R10 mm	days	Frequency related (FR)
Number of very heavy precipitation days (count of days when precipitation is ≥20 mm)	R20 mm	days	
Annual maximum consecutive dry days (<1 mm)	CDD	days	Duration related (DR)
Annual maximum consecutive wet days (>1 mm)	CWD	days	
Wet day precipitation (total precipitation in wet days)	PRCPTOT	mm	General (GN)
Wet days (count of days when precipitation is ≥1 mm)	WD	days	
Simple daily intensity index (Average precipitation on wet days)	SDII	mm/day	

The non-parametric Pettitt test is commonly used to detect structural changes in data. We applied the method to find significant change points in precipitation series (Pettitt, 1979).

2.4.2. Extreme Precipitation Indices

Extreme Precipitation Indices are one of the most widely used precipitation indices. This series of precipitation indices provides a more comprehensive picture of multiple aspects of precipitation, such as intensity, frequency, and duration of extreme events. The temporal and spatial analysis of these extreme precipitation indices in Nepal could provide a comprehensive understanding of extreme precipitation in this country. In this study, we adopted all the 11 extreme precipitation indices for analysis of change in precipitation (Table 1), and divided them into four terms: High-Intensity-Related (HIR), Frequency-Related (FR), Duration-Related (DR), and General (GN) indices. HIR indices (RX1day, RX5day, R95pTOT and R99pTOT), in the unit of mm, reflect the precipitation amount during the extreme precipitation events. RX1day and RX5day represent the maximum precipitation amount for 1 and 5 consecutive days, respectively. R95pTOT and R99pTOT represent the total precipitation amount of the daily precipitation greater than the 95% and 99% percentile. FR indices, in the unit of day, revealing the frequency of extreme events. They include R10 mm and R20 mm that are the number of days with daily precipitation amount greater than 10 and 20 mm, respectively. DR indices are CDD and CWD that reflect the maximum consecutive dry and wet days, respectively, in the unit of day, indicating the length of dry and wet seasons. Lastly, GN includes PRCPTOT (mm), SDII (mm/day) and WD (day), representing the total precipitation in a year with rainy days (daily precipitation>1 mm/day), the annual average daily precipitation intensity, and the number of days in a year with rainy days.

The Indice Calculation CLIMate (ICCLIM) package in Python 3.0 (Scussolini et al., 2019) was employed for calculating extreme indices based on gridded data. The RClimDex software package in R Statistical Software was used for the calculation of indices on station data, recommended by The Expert Team on Climate Change Detection and Indices (https://etccdi.pacificclimate.org/software.shtml) (Zhang et al., 2011). The Rclimdex's screening criteria for the data are the same as ours, therefore the extreme precipitation indices for the missing measurement year will not be exported.

2.4.3. Bias-Correction Methods

Two linear correction methods were used to perform bias correction in our study (Luo et al., 2020). The linear scaling (LS) method uses the ratio between the mean monthly observations and the corresponding estimates to correct APHRODITE. Specific equations are as follows:

$$P^{*}_{\mathrm{APH}}(d) = P_{\mathrm{APH}}(d) \cdot \left[\frac{u_m(P_{\mathrm{DHM}}(d))}{u_m(P_{\mathrm{APH}}(d))}\right] \tag{9}$$

where $P_{\mathrm{APH}}(d)$ and $P^{*}_{\mathrm{APH}}(d)$ are daily APHRPDITE data before and after correction, $P_{\mathrm{DHM}}(d)$ is daily station observation data, and $u_{\mathrm{m}}\ (P_{\mathrm{APH}}(d))$ and $u_{\mathrm{m}}\ (P_{\mathrm{DHM}}(d))$ are monthly averages of APHRIDTE and observation data in month m, respectively.

The local intensity scaling (LIS) method first requires determining an adjusted precipitation threshold (P_{th}, APH) such that the number of days in APHRODITE greater than this threshold matches the number of observed days with precipitation greater than 0 mm. Next, a linear scaling factor (s) is calculated for wet days:

$$s = \frac{u_m(P_{\mathrm{DHM}}(d)|P_{\mathrm{DHM}}(d) > 0\ \mathrm{mm})}{u_m(P_{\mathrm{APH}}(d)|P_{\mathrm{APH}}(d) > P_{\mathrm{th,APH}}) - P_{\mathrm{th,APH}}} \tag{10}$$

where $u_m\ (P_{\mathrm{DHM}}(d)|P_{\mathrm{DHM}}(d) > 0\ \mathrm{mm})$ is the monthly average precipitation for observations with daily precipitation greater than 0 mm. $u_m\ (P_{\mathrm{APH}}(d)|P_{\mathrm{APH}}(d) > P_{\mathrm{th,APH}})$ is the monthly mean precipitation in APHRODITE for precipitation greater than the threshold P_{th}, the corrected precipitation is then as follows:

$$P^{*}_{\mathrm{APH}}(d) = \max(s \cdot (P_{\mathrm{APH}}(d) - P_{\mathrm{th,APH}}), 0) \tag{11}$$

3. Results

3.1. Long-Term Trends: Temporal Patterns of Extreme Precipitation Indices

Indices were divided into four groups to reflect each aspect of extreme precipitation: High-intensity-related (HIR) indices including RX1day, RX5day, R95pTOT, and R99pTOT, Frequency-related (FR) indices including R10 mm and R20 mm, Dry and Wet Spell or duration-related (DR) indices including CDD and CWD, and general indices including PRCPTOT, SDII, and WD. The temporal trends of these indices in the two data sets are compared and illustrated (Figure 2).

3.1.1. A Drying Trend of Extreme Precipitation

Both DHM and APHRODITE data sets exhibited a consistent drying trend in extreme precipitation indices from 1971 to 2015. This tendency was evident in most indices, including HIR and FR indices (Figure 2). In APHRODITE time series, there are 2 out of 4 HIR indices demonstrating statistically significant weakening trend based on modified Mann–Kendall trend analysis at 90% confidence level. They are RX1day and R99pTOT, with Theil–Sen's slope values are 0.095 mm per year, and −0.838 mm per year, respectively. Max 1-day precipitation amount (RX1day) reduced by 7.0%, and total precipitation of days in >95th percentile and in >99th percentile reduced by 11.2%, and 20.0%, respectively. Both FP indices show significantly reduced trends, by 5.9% in R10 mm from 43 to 41 days, and by 11.6% in R20 mm from 15.5 to 13.5 days. However, both DR indices are found to have a significant increasing trend since 1971, illustrating both the increases in the annual longest dry spells (CDD) from 50 to 55 days (or 10%), and the annual longest wet spells (CWD) from 45 to 55 days (or 22%). In contrast, the annual total precipitation amount (PRCPTOT), the average precipitation intensity (SDII), and wet days (WD) of general indices show non-significant change during the period.

Furthermore, the DHM in-situ data set time series confirms the drying tendency over Nepal. It shows a descending trend in extreme precipitation indices of intensity and frequency, and an ascending trend in indices of duration. Among them, 2 out of 4 HIR indices showed significant weakening trend (RX1day and R99pTOT, same significant indices with APHRODITE). 1 out of 2 FR indices showed significant descending trend (R10 mm) as well as all duration indices have significant trends. But the slopes of DHM indices trends are much gentler than APHRODITE. For example, R10 mm in FR indices passes 95% significant level, reduced by 3.8% from 53 to 51 days. Meanwhile, consistently increasing results in DR indices are also found in DHM data sets. CDD increased by 29.0% from 62 to 80 days, and CWD increased by 21% from 14 to 17 days. For the general indices, a significant reduction is found in WD that does not exist in APHRODITE.

3.1.2. Decadal Variability and Turning Point in 2003

Apart from the long-term descending trends, Nepal also experienced strong decadal variability in extreme precipitation indices from 1971 to 2015. Both data sets revealed strong decadal variability in extreme precipitation

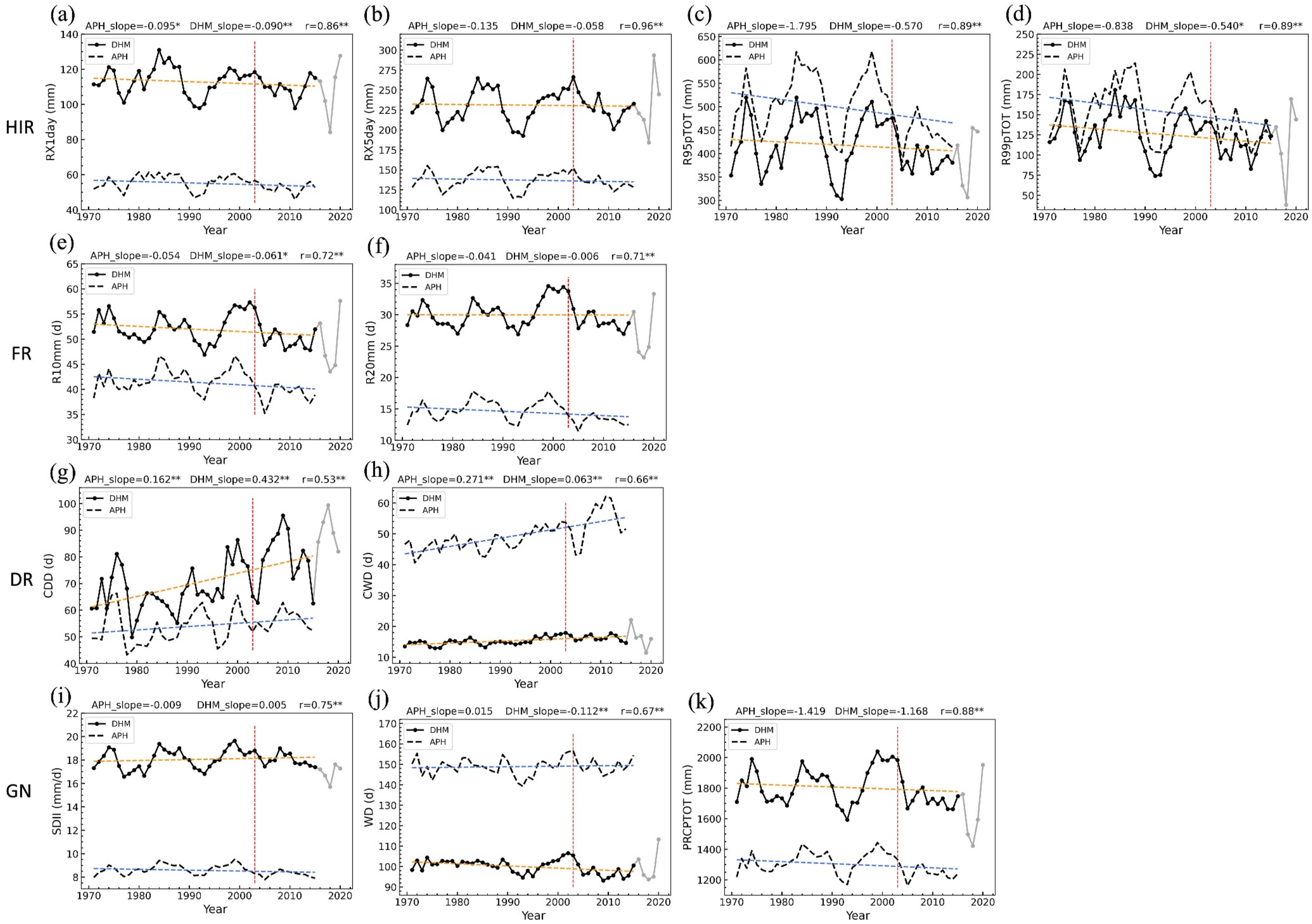

Figure 2. Time series of extreme precipitation indices (listed in Table 1) for DHM in-situ data (dotted line) and APHRODITE (dashed line) from 1971 to 2015 in Nepal. Linear trend lines are represented by yellow (DHM) and blue (APHRODITE) dashed lines. The red vertical line denotes the turning point year of 2003.

indices, with wet decades occurring in the 1980s and late-1990s to early-2000s, and dry years in 1979, 1992, 2007, 2009, and 2011. The similarity in decadal patterns between the data sets underscores the robustness of these findings.

A significant turning point in extreme precipitation trends was detected in both DHM and APHRODITE data, occurring around 2003 over the 45-year study period. There are 8 (6) out of 11 extreme precipitation indices in APHRODITE (DHM) found around this turning point, including HIR indices, FR indices, and general index (Table 2). Results show the shift from a relatively higher level of extreme precipitation to a lower level in these extreme precipitation indices. In addition, the mean value of the annual WYI was 0.15 before 2003 and –0.08 after 2003. The monsoon WYI also turned from positive to negative before and after 2003. Similar results were also found in IMI index (0.25 to −0.23) and SASMI index (−0.04 to −0.45). It indicates a significant shift from strong to weak intensity of the monsoon before and after years around 2003. This high-to-low shift corresponds well with the extreme precipitation indices mentioned above. In fact, this turning point is very close to the point in 2002 that was found by J. Jiang, Yi, et al. (2023) and Jin and Wang (2017) in the region near Nepal. Jin and Wang (2017) found in Central India, there is a revival of precipitation after 2002 since the long period of low-level precipitation since the 1950s. J. Jiang, Yi, et al. (2023) discovered that in the southern Tibetan Plateau, precipitation shifts from a higher amount to a lower amount at the turning point around 2002. This alignment in turning points suggests a common influence, possibly related to changes in South Asia Monsoon circulation and external factors like temperature contrasts and aerosols. Both precipitation and extreme precipitation in Nepal may be affected by the circulation change under the large background.

10.1029/2024EA003563

Table 2
Detected Turning Points for Each Extreme Precipitation Index and Monsoon Indices as Determined by the APHRODITE and DHM Data Sets

	Extreme precipitation indices	APHRODITE	DHM
HIR	RX1day	**2003**	1988
	RX5day	**2008**	**2008**
	R95pTOT	**2002**	**2004**
	R99pTOT	**2003**	1988
FP	**R10 mm**	**2002**	**2004**
	R20 mm	**2002**	**2004**
DR	CDD	1988	1997
	CWD	1994	1996
General	SDII	**2001**	2010
	WD	1995	**2004**
	PRCPTOT	**2003**	**2004**
	Monsoon Indices	Turning point of Monsoon Indices	
Annual	**WYI**	**2001**	
	IMI	1997	
Monsoon season	**WYI_JJAS**	**2001**	
	IMI_JJAS	**2007**	
	SASMI	**2008**	

Note. Bold items indicate turning points around 2003, with values both earlier and later by 5 years.

3.1.3. Comparison Between APHRODITE and DHM

Prior to comparing the two data sets, we note that the DHM data are from the stations located below 3,000 m and the time series could only provide extreme precipitation information in low-to-middle elevated regions. However, APHRODITE data set covers the entire country, although the values in high elevated regions may have large uncertainties. More details can be found in Section 2 Methodology and Data set. The time series of the two data sets illustrate consistent results of most indices with correlation coefficient values exceeding 0.6 (except CDD). It indicates the low-to-middle region (DHM data representative) overall shares similar trends and variations with the entire country (APHRODITE representative). The absolute differences may come from the data set's differences or from the elevation representatives. Our further analysis of spatial pattern comparison has a more comprehensive analysis between the two data sets based on the same location (Section 3.2).

Combining all extreme precipitation indices trends in APHRODITE, we can summarize that extreme precipitation became weakened in terms of both intensity and frequency, although the overall precipitation does not show any significant trends in Nepal as a whole. However, it appears that the precipitation variability has become larger over time as indicated by both increased durations of maximum dry period and maximum wet period.

3.2. Spatial Patterns of Extreme Precipitation Indices

3.2.1. Extreme Precipitation Trends

As evident from the long-term time series, extreme precipitation exhibits weakening trends in intensity and frequency indices while showing enhancing trends in duration. These statistically significant changes in extreme precipitation are characterized by spatial heterogeneity. Over a 45-year study period, the spatial trends of the HIR and FR are segmented into full stage and two stages: Stage I (1971–2003) and Stage II (2004–2015), respectively (Figure 3).

In the full-time stage, both data sets consistently show significant reduction trends over most parts of the country (east of 81°E). However, several pockets with substantial increasing trends emerge, notably in the western region (80°–81°E), southwestern Terai (80°–83°E, 27.5°–29.0°N), central Siwaliks and Middle Mountains (~84°E, 27.5°–28.5°N), southeastern Terai (85°–86°E, 26.5°–27.5°N), and eastern High Himalayas (85°–87°E, 28°–

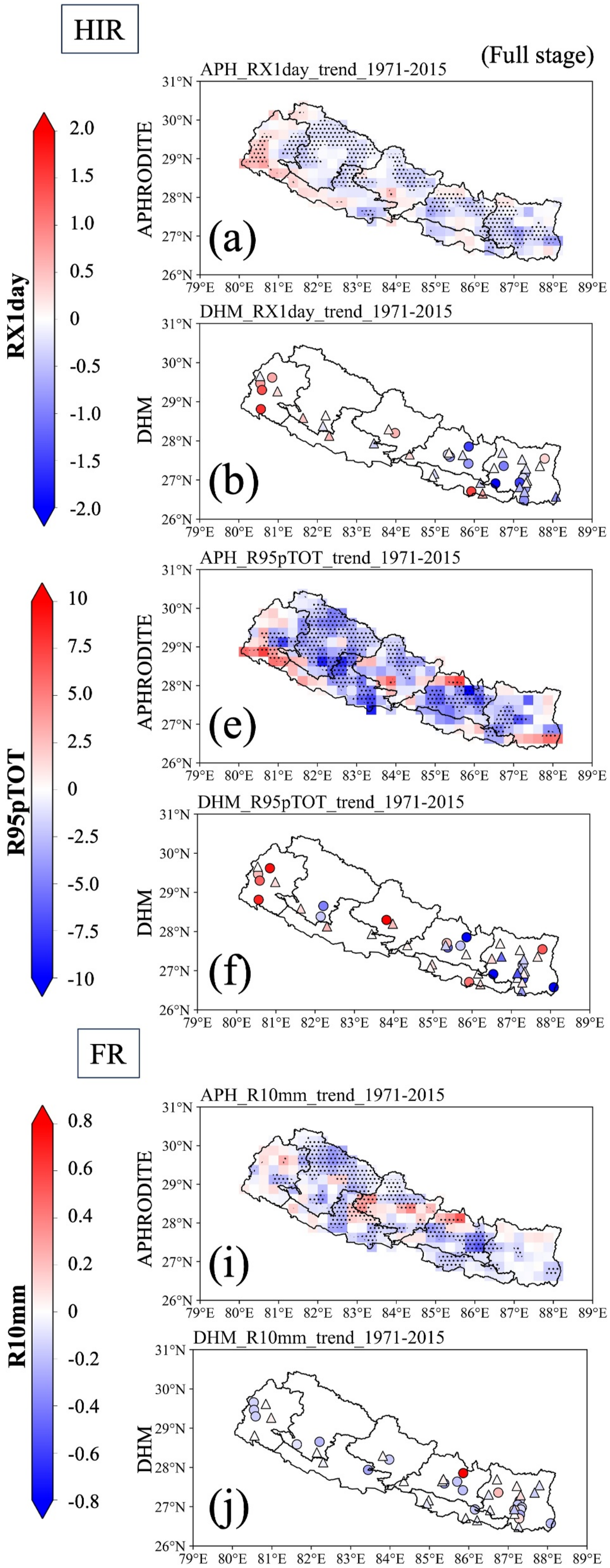

Figure 3. Spatial pattern of trends in intensity (RX1day, RX5day, R95pTOT, R99pTOT) and frequency (R10 mm, R20 mm) extreme precipitation indices during the entire period 1971–2015. Dotted areas in APHRODITE and solid circles in DHM in-situ data indicate significance at 90% confident level; triangles in DHM denote non-significant trend stations. Trend analysis used Mann-Kendall test and Theil-Sen slope estimation method. The temporal trend and its significance at each station and each grid was calculated to form the spatial distribution.

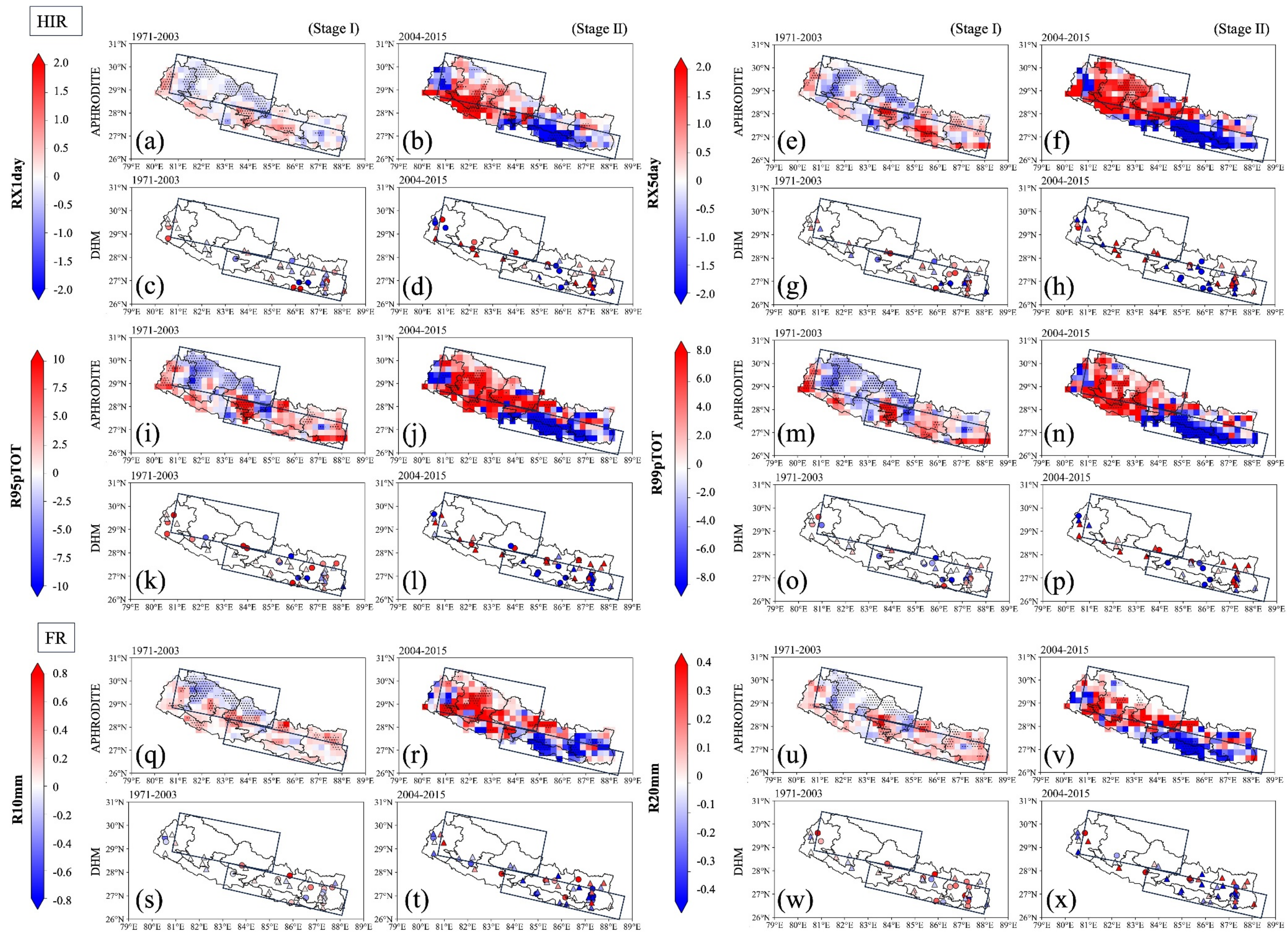

Figure 4. Similar to Figure 3, but for stage I and II, respectively.

28.5°N) (Figure 3). Similar patterns are observed in SDII and PRCPTOT of the general-related indices (Figure S10 in Supporting Information S1). The pattern WD is a bit different. It shows a distinct pattern of pronounced contrast in trends, transitioning from substantial increases to significant decreases, with the division occurring at 85°E. Regarding the DR indices, CDD and CWD generally exhibit increasing trends across the country, corresponding to the temporal increasing trends. These two indices show opposing signs in similar regions in the western high-elevated areas (81°–83°E, 28.5°–30.5°N) and most of the Terai region where CDD shows significant reductions while CWD indicates increases during the full stage (Figure S10 in Supporting Information S1). However, both CDD and CWD exhibit increases in the eastern High Himalayas.

This overall declined trend with the western region increases in extreme precipitation spatial pattern is also mentioned in studies by Bohlinger and Sorteberg (2018), Karki et al. (2017), and Talchabhadel et al. (2018). In particular, Bohlinger and Sorteberg (2018) used 98 stations to detect the extreme precipitation trends during 1971–2010 over Nepal. They also found a substantial increase in extreme precipitation in Far-west Nepal (80°–81°E). This matches very well with what we observed on both the station data and the APHRODITE grid data set, again demonstrating the accuracy of APHRODITE.

3.2.2. Consistency Between the Two Data Sets

The study demonstrates consistency between the DHM and APHRODITE data sets in terms of long-term trends and spatial patterns (Figures 3 and 4, S10 and S11 in Supporting Information S1). The correlation coefficient between the two data sets is generally high in the overlapped area (Figure S5 in Supporting Information S1). It is worth noting that specific discrepancies between the DHM and APHRODITE data sets are found in CWD and

WD indices. The relative bias and RMSE maps (Figures S6 and S7 in Supporting Information S1) support the overall consistency in most indices between the two data sets and share similar issues in CWD and WD. Certain discrepancies exist in extreme precipitation indices between the two data sets over the same location. For example, APHRODITE data set shows larger values in R95pTOT and R99pTOT in HIR, CWD in DR and WD in GN, compared with station data set. But it underestimates values in the other seven indices, indicating an overall drier condition in APHRODITE in low-to-middle elevated regions where most station is located. Despite these differences, the overall trends and variations align between the two data sets in the overlapped regions, strengthening the robustness of the findings.

Meanwhile, we also found APHRODITE data are good at lower altitude but has larger bias to the station data at high altitude region (above 2,000 m). There are 8 out of 11 extreme precipitation indices showing a larger bias over the high altitude region. These indices include: RX1day, RX5day, R95pTOT, R99pTOT, R10 mm, R20 mm, PRCPTOT, and SDII (Figure S8 in Supporting Information S1). The relative biases in these indices are larger in the high altitude region by around 5%–10% compared with them over the low altitude region. Accordingly, we added a correct factor to trim the APHRODITE precipitation to the DHM station data, for the target of reducing bias in the high altitude region in Nepal. We adopted two classic linear correct methods LS and LIS (Section 2.4.3) and effectively reduced the bias. Taking R95pTOT index as an example, the relative bias over the high elevated region is around −30% when comparing APHRODITE to the station DHM data. Using the two correct methods LS and LIS, relative bias reduced to 2% and −5%, respectively. For all other extreme precipitation indices, these two methods can significantly have reduced the relative bias. However, the correction methods did not change the spatial or temporal trends. The trends of most of the indices are consistent before and after using the two correct methods (Figure S9 in Supporting Information S1), indicating the consistent temporal and spatial results.

3.2.3. Recent Western (81°–85°E) Revival of Extreme Precipitation

Despite the long-term drying trend found in both data sets, there are distinguishing patterns in the two stages. In stage I, most indices of HIR, FR, and GN illustrated the northwest decline and southeast increase trends. But the spatial pattern switched in stage II with northwest increase and southeast reduction trends over very similar regions (Figures 4 and S11 in Supporting Information S1). In particular, the western region (81°–85°E) had significant reductions from 1971 to 2003 but then underwent a significant enhancement from 2004 to 2015, indicating a western revival. This revival, marked by increasing extreme events, challenges the overall drying trend observed in earlier years. On the other hand, the southeastern region (83°–88°E, 26°–28°N) has experienced first wetting and then drying trends during stage I and stage II, with less risks of extreme precipitation for the past few years. In fact, the long-term spatial trend 1971–2015 is the combination of the two stages and forms the overall drying tendency of most of the region.

This phenomenon has also been detected in many regions of the planet, highlighting the complex nature of extreme precipitation trends and spatial variation (Bohlinger & Sorteberg, 2018; Caesar et al., 2011; D. Shrestha et al., 2021; N. K. Shrestha, Qamer, et al., 2017; Pandey et al., 2021). Yao et al. (2020) used the ensemble mean of seven precipitation data sets and found a South Drying–North Wetting dipole pattern in precipitation trends over the Hindu Kush–Karakoram–Himalayan region from 1980 to 2018. Precipitation reduced over the south drier trend region was found at the rate of around 2.6 mm per year. Nepal is geologically next to the southern region and the precipitation reduced at around 1.4 mm per year using APHRODITE (DHM at around 1.2 mm per year) during a similar period. More locally, Pokharel et al. (2020) also using the APHRODITE data set, noted a west-reduction-east-increase division in extreme precipitation in Nepal for the period of 1981–2007. Such a spatial pattern was also confirmed in our study for a longer study period (1971–2015). Furthermore, Duncan et al. (2013) using APHRODITE only, also found the total and monsoon extreme precipitation in most parts of Nepal, except the central belt and the Terai in the central and eastern parts of the country, showed a downward tendency from 1950 to 2007. The result provides additional information before 1971, indicating the decreasing trend has been existing for nearly 60 years. Notably, we provide an updated analysis of recent years, revealing a transition from the previously descending pattern to a west revival-east reduction pattern in extreme precipitation.

Table 3
Correlation Coefficients Between Monsoon Index and Extreme Precipitation Indices During 1971–2015 After 3-Year Moving Average

		Annual				JJAS					
		WYI		IMI		WYI		IMI		SASMI	
		APH	DHM	APH	DHM	APH	DHM	APH	DHM	APH	DHM
HIR	RX1day	0.36**	0.34**	−0.03	−0.11	0.38**	0.24	0.00	−0.19	−0.15	−0.09
	RX5day	0.46**	0.54**	−0.06	−0.08	0.25	0.17	−0.05	−0.12	0.00	−0.02
	R95pTOT	0.55**	0.63**	−0.05	0.01	0.47**	0.26	0.10	−0.03	−0.07	−0.01
	R99pTOT	0.38**	0.55**	−0.09	−0.18	0.45**	0.21	0.08	−0.17	−0.22	−0.03
FR	R10 mm	0.67**	0.71**	−0.03	−0.10	0.49**	0.38**	0.12	0.13	0.31**	0.08
	R20 mm	0.65**	0.67**	−0.04	0.11	0.48**	0.29*	0.10	0.13	0.27*	0.01
DR	CWD	0.01	0.36**	0.22	0.48**	−0.59**	−0.27*	−0.41**	−0.12	0.01	0.11
	CDD	0.17	−0.13	0.63**	0.54**	−0.11	−0.44**	0.09	−0.02	0.08	−0.34
GN	SDII	0.53**	0.64**	0.01	0.14	0.41**	0.01	0.09	−0.15	−0.07	−0.03
	WD	0.52**	0.12	0.15	−0.14	0.04	0.60**	−0.07	0.34**	0.34**	0.15
	PRCPTOT	0.67**	0.69**	0.00	0.02	0.48**	0.35**	0.12	0.09	0.18	0.11

3.3. Mechanisms Behind the Extreme Precipitation Change

3.3.1. Insights From Large-Scale Monsoon Circulation

Although there is considerable regional variability within the topographic domain, we first address the national-scale temporal pattern of extreme precipitation, as opposed to regional or local characteristics. We first focalize on large-scale monsoon circulation indices that assess the strength of the South Asia Summer Monsoon. These indices (WYI, IMI, and SASMI) may serve as crucial linkages between extreme precipitation and the broader-scale circulation patterns, thereby unraveling potential local and nonlocal influences on the extreme precipitation.

In Table 3, we have computed correlation coefficients between large-scale circulation indices and extreme precipitation metrics, providing crucial insights into their relationships. Notably, the WYI index stands out with the highest correlation values, most of which are statistically significant. For example, the WYI index shows a strong positive correlation with HIR and FR extreme precipitation metrics for both data sets, such as RX1day (0.36** and 0.34** for APHRODITE and DHM, respectively), RX5day (0.46** and 0.54**), R95pTOT (0.55** and 0.63**), R99pTOT (0.38** and 0.55**), R10 mm (0.67** and 0.71**), and R20 mm (0.65** and 0.67**). These findings underscore the significant impact of the broader Asian monsoon, as measured by the WYI index, on extreme precipitation in Nepal.

The IMI index demonstrates significant associations with DR metrics related to duration, including strong correlations with CDD (0.63** and 0.54** for APHRODITE and DHM, respectively) and CWD (0.48** for DHM). In contrast, SASMI primarily shows connections with frequency-related metrics, positioning it as the least influential among the monsoon indices. The robust link between large-scale monsoon indices and extreme precipitation underscores the key contribution of dynamics in shaping extreme precipitation events. However, IMI exhibits a weaker correlation with extreme precipitation, potentially due to its focus on lower-level winds alone. SASMI is restricted to the monsoon months offering limited insights for Nepal and does not distinguish itself when compared to the other two indices within the context of the monsoon months (Table 3).

During the period from 1971 to 2015, a consistent weakening trend in both WYI and SASMI (Figure 5) is evident. This aligns with prior studies emphasizing declining monsoon circulation. The Indian monsoon has, since the 1980s, notably weakened by 5.4% per decade ($P = 0.01$) (Turner & Annamalai, 2012; Yao et al., 2012). The weakening of the monsoon circulation would impact the frequency and intensity of synoptic and para-synoptic phenomena, which includes low pressure systems, mesoscale-convective systems and thunderstorms that can trigger extreme precipitation in Nepal. For example, the number of low-pressure systems over the Bay of Bangle declined significantly that can potentially move north-northwestward to Nepal and can result extreme precipitation there (Figure S12 in Supporting Information S1). Diminishing Indian monsoons have also reduced the

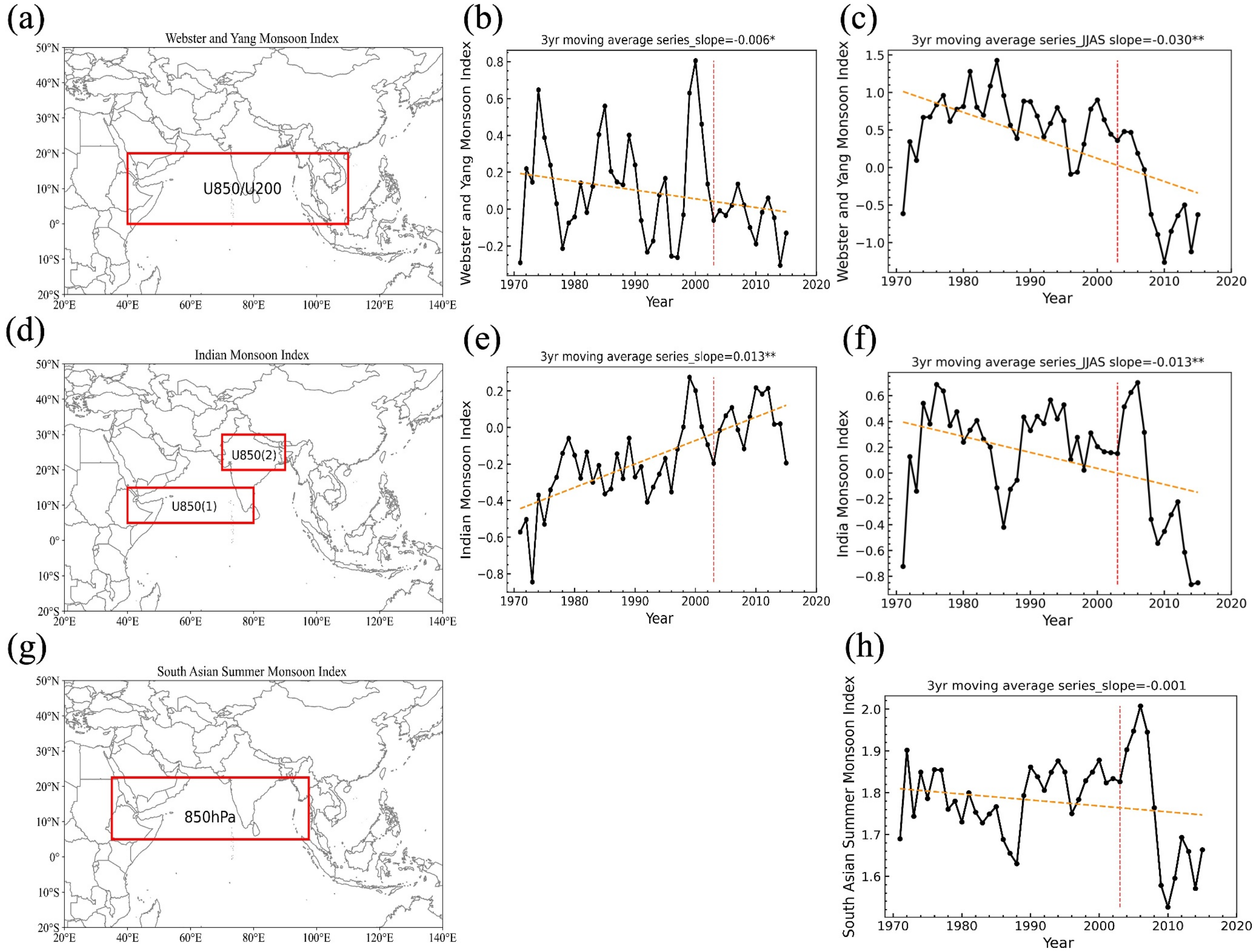

Figure 5. Left Panel: Schematic maps illustrating the definition of monsoon indices, including WYI, IMI, and SASMI. Boxes indicate regions where zonal winds are utilized to define the monsoon indices. Central Panel: Time series depicting the annual monsoon index. Right Panel: Time series showing the JJAS monsoon index.

amount of moisture drawn from the tropical oceans of the Indian subcontinent, potentially reducing precipitation in Nepal which relies heavily on upslope moisture transport to the Himalayas. Furthermore, the turning point is also detected in the three monsoon indices (Table 2). Results show that WYI, WYI monsoon, IMI monsoon and SASMI monsoon all has a turning point around 2003. This further reinsures the critical role of the monsoon indices on extreme precipitation long-term trend.

Atmospheric moisture plays a critical role in extreme precipitation events. We have expanded our analysis to include the moisture flux across all vertical layers in Nepal, utilizing ERA5 data. Temporal and spatial patterns were examined, revealing important connections between moisture flux and extreme precipitation patterns. The climatology of moisture flux indicates a strong atmospheric moisture stream originating from the Arabian Sea, passing through central India, and reaching the Bay of Bengal before turning westward into Nepal (Figure S15b in Supporting Information S1). This stream provides the necessary moisture for extreme precipitation events in Nepal, with changes in this stream correlating with shifts in extreme precipitation patterns.

We conducted a time series analysis of integrated water vapor transport fluxes over Nepal from 1971 to 2015, revealing a slight but not statistically significant increase (Figure S15a in Supporting Information S1), which corresponds with local temperature changes via the Clausius-Clapeyron (C-C) relationship. However, this does not fully explain the reduction in extreme precipitation observed over the period. In fact, the study period shows a weakening of the monsoon circulation, as indicated by the WYI. This weakening, combined with increased moisture transport, resulted in an overall reduction of extreme precipitation in Nepal, underscoring the dominant role of dynamic factors.

The diminished monsoon circulation results from various factors, including Indian Ocean warming, more frequent and intense El Niño events, anthropogenic aerosols, and land use changes across the subcontinent (J. Jiang, Yi, et al., 2023; Mishra et al., 2012; Roxy et al., 2015; Saha et al., 2014; Singh et al., 2019). Roxy et al. (2015) previously proposed that the primary cause of weakened monsoonal circulation lies in reduced temperature gradients between land and sea in the South Asian Summer Monsoon region. From 1950 to 2015, summer monsoon rainfall markedly reduced in central-eastern and northern India, as well as the Himalayan foothills, due to reduced tropospheric thermal contrast. In particular, the rapid warming of the Indian Ocean, plus the relatively feeble warming of the subcontinent, has weakened the land-sea heat contrast and ultimately damping the summer monsoon, Hadley circulation, and south-westerlies, leading to less rainfall across various South Asian regions (Roxy et al., 2015).

The east-west difference in the Indian Ocean SST, quantified by the IOD index, is also a critical factor in the South Asian monsoon circulation. Its temporal trend and turning point were analyzed here for deeper understanding the mechanisms driving the monsoon and extreme precipitation change in Nepal. Results showed that from 1971 to 2015, both annual and monsoon IOD indices illustrated significant increasing trend ($p < 0.05$), with negative phase shifting to positive phase (Figure S13 in Supporting Information S1). Such a change results in a weakening of the low-level westerly (Figure 6e) that can further weaken the strength of monsoon circulation, and reduce evaporation of moisture from the east ocean. Both of which are unfavorable for precipitation. In addition, the turning points detection results showed that the IOD index changed from negative to positive in 2003 (annual round index: −0.131 to 0.03; monsoon seasonal index: −0.151 to 0.010). The same turning point strongly suggests that in 2003, the IOD changes its phase from negative to positive, resulting in monsoon circulation changes from higher to lower intensity and extreme precipitation changes from higher to lower levels at the turning point of 2003.

3.3.2. Local Wind Impacts

We further examined the regional extreme precipitation pattern over Nepal using local-scale wind fields at three representative atmospheric levels: 850 hPa, 500 hPa, and 200 hPa. We also analyzed the spatial patterns of the integrated moisture transport fluxes and performed a moisture budget analysis across Nepal's boundaries. Since the bulk of the precipitation (about 80% of the annual total) occurs in monsoon season (June–September), in this section, and contrasted wind fields during summer and winter monsoon seasons, we highlight the summer monsoon JJAS averages and characterize the spatial trends over Nepal. We also separate the analysis into Stage I and Stage II based on the distinct signals observed over Nepal, which may be attributed to contrasting atmospheric processes.

At the 850 hPa level, wind in the climatology illustrates an elongated low pressure belt along the Indo-Gangetic plains that is commonly referred to as the monsoon trough during the summer monsoon season (JJAS) (Figure 6). The low-level southwesterly branch over North India and southeasterly branch near Nepal provide a pivotal contribution to the mean monsoon rainfall and provide water vapor for the formation of extreme events in the region. At the 500 hPa level, the monsoon trough extends from the Arabian Sea to the foot of Himalaya where a low-pressure system is observed. The wind patterns align with cyclonic circulation within the low-pressure region at the 500 hPa level. At the 200 hPa level, a strong anticyclone known as the South Asian High is present over Nepal and the southern Tibetan Plateau during the summer months (Mason & Anderson, 1963), which can provide an upper-air pumping effect through a divergence center. Any change in the circulation of the upper atmosphere would directly modulate the divergent pumping effect, which would further affect the intensity of the upward movement over Nepal (Liu et al., 2013). The tropical easterly jet and the subtropical westerly jet are located on the southern and northern flanks of the South Asian High, respectively (Figure 6).

During stage I (1971–2003), the monsoon trough at the 850 hPa level intensified notably in south-southeast of Nepal (Figure 6b), driven by changes at higher atmospheric levels (500 hPa and 200 hPa), which we detail in the later paragraphs in this section. Concurrently, moisture transport fluxes increased significantly in these regions and formed a cyclonic trend of the moisture fluxes (Figures S15e and S15h in Supporting Information S1), leading to a localized increase in extreme precipitation over south and southeast of Nepal.

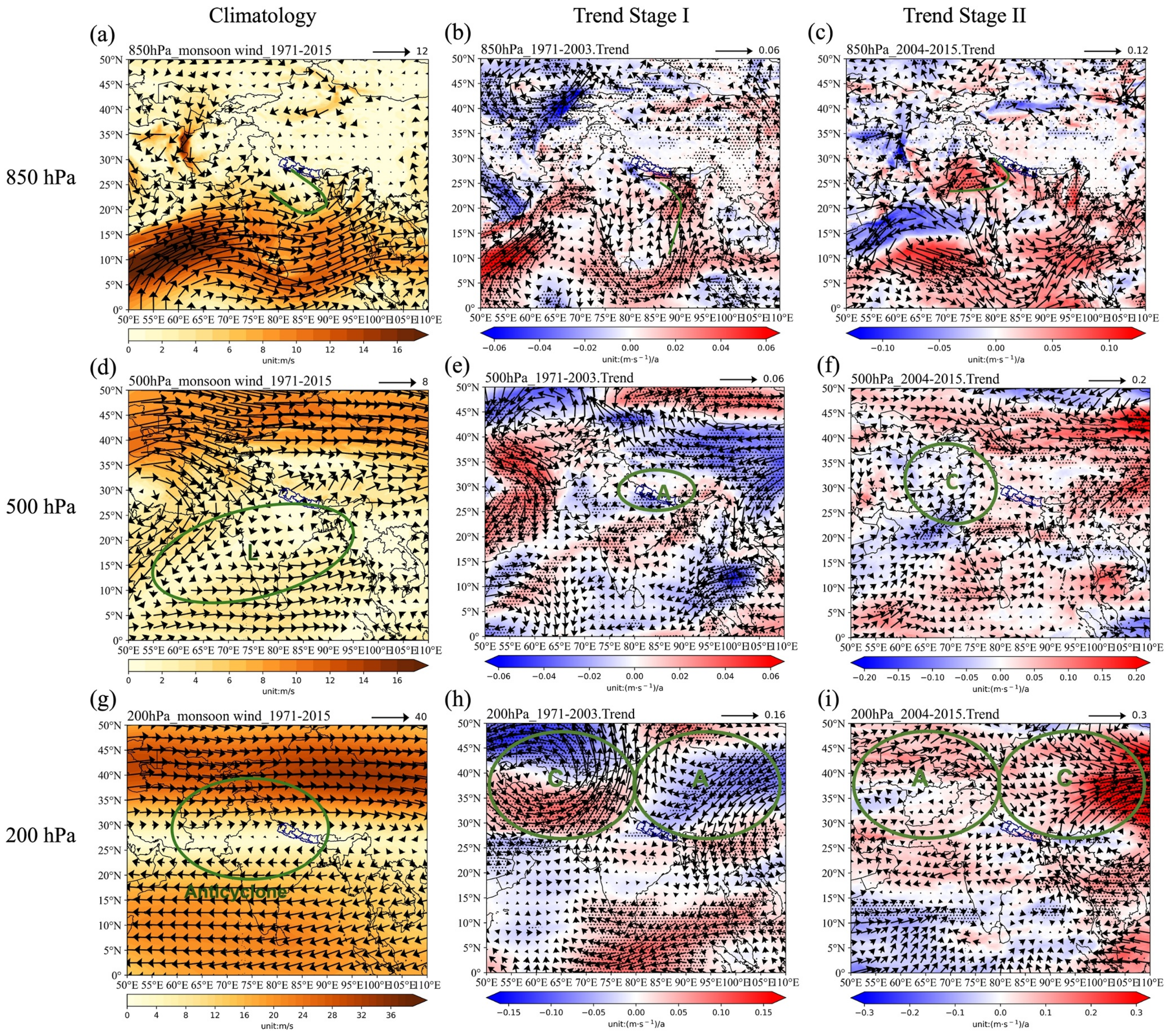

Figure 6. Climatology (left panel) and trends of wind fields at the 850 hPa, 500 hPa, and 200 hPa levels during the summer monsoon (JJAS) season during 1971–2015. Trends are separately shown for Stage I (middle panel) and Stage II (right panel). Data source: ERA5 reanalysis data (Hersbach et al., 2023a). C is short for cyclonic circulation, and A is for anticyclonic circulation.

In stage II, the monsoon trough intensified over westward Nepal (Figure 6c), influencing western Nepal with more pronounced dynamic uplift, while moisture transport fluxes exhibited a slight increase (Figures S15f and S15i in Supporting Information S1). These changes, alongside enhanced moisture influx at the western boundary, contributed to the observed increase in extreme precipitation in western and southwestern Nepal.

It also worth to mention that, moisture budget analysis further supports the distinct spatial patterns during stages I (western reduction) and II (western increase). We found that moisture budget illustrates an enhanced moisture income at the western boundary and a net increase of moisture at the west-east direction in Nepal in stage II (Figures S15f and S15i in Supporting Information S1), potentially contributing the increase of extreme precipitation over western Nepal. The moisture patterns observed during stages I and II, combined with changes in monsoon circulation, correlate well with the observed changes in extreme precipitation, providing valuable insights into the mechanisms in Nepal.

The monsoon trough shift is largely driven by changes in the upper levels. During stage I, an anticyclonic circulation tendency was observed at the 500 hPa level over Nepal (Figure 6e). This circulation pattern is not conducive to precipitation formation, as it tends to induce downward motion, contributing to an overall reduction in precipitation across Nepal. This trend extends to 850 hPa, forcing the monsoon trough to migrate southward (Figure 6b), resulting in reduced precipitation in north and west regions, but increased precipitation in southeast regions. Under this circulation background, the moisture transport fluxes also contribute to extreme precipitation changes locally.

We also examined circulation changes at the 200 hPa level, where the South Asia High's anticyclonic circulation typically supports upper-level divergence and associated uplift. However, during stage I, a significant upper-level cyclonic-anticyclonic anomalies developed along the northern edge of the South Asia High, weakening the upper-level westerlies over Nepal (Figure 6h). These circulation patterns could drive changes in the lower levels, leading to anticyclonic trends at 500 hPa and more divergent conditions at 850 hPa and suppressing precipitation.

In stage II, the circulation patterns at each vertical level showed localized differences. At 500 hPa, a significant cyclonic circulation trends persisted on the west of Nepal (Figure 6f). At 850 hPa, the circulation remained cyclonic, causing the monsoon trough enhanced westward, which, coupled with increased moisture transport, resulted in heightened precipitation in western Nepal. Up to 200 hPa, there is an upper level anticyclonic-cyclonic pattern change on the northern border of the climatology South Asia High (Figure 6i). It results in cyclonic changes at 500 hPa over the western Nepal that could potentially increase precipitation there.

3.3.3. Other Factors Contributing to Extreme Precipitation

Changes in precipitation extremes are determined by warming-induced changes in atmospheric motion dynamic and thermodynamic processes. Precipitation extremes are also influenced by regional forcings and feedbacks like land use and aerosol forcings, soil moisture-temperature feedbacks, soil moisture-precipitation feedbacks, and snow/ice-albedo-temperature feedbacks (Jia et al., 2019; Lorenz et al., 2016; Seneviratne et al., 2021; Zhili Wang, Duan, et al., 2017; Wang, Lin, et al., 2017). However, in state-of-the-art Earth System Models (ESM), there is only an intermediate level of confidence in the representation of the processes involved. The above-discussed large-scale and local-scale atmospheric dynamic changes are based on observations. Indeed, climate models consider dynamic contributions to strongly alter the change rate of extreme precipitation, but these vary considerably from model to model and are more uncertain than thermodynamic contributions (Pfahl et al., 2017; Seneviratne et al., 2021; Shepherd, 2014; Trenberth et al., 2015).

In terms of the thermodynamic contribution, it often plays an almost uniform role based on the theoretical C-C rate. Observational studies have shown that at the global scale from 1950 to 2018, for every 1°C increase in global mean surface temperature, extreme precipitation increases by about 7% that meets the theoretical value of the C-C rate (Fischer & Knutti, 2015; Sun et al., 2021). In the South Asia Monsoon region, thermodynamic contribution was found to play a less important role to extreme precipitation compared with the dynamic forcing from Indian monsoon and local-scale circulation by many previous studies (e.g., Gao et al., 2018; Wang, Duan, et al., 2017; Wang, Lin, et al., 2017). In fact, our results found the RX1day reduction and the temperature increase in Nepal during 1971–2015 (Table 4). The RX1day reduction in Nepal implies that thermodynamic warming did wet the local atmosphere over Nepal, but it did not lead to an actual rise in extreme precipitation. In contrast, a weakening of the monsoon circulation and local-scale circulation may play a dominant role in the extreme precipitation reduction. This is also consistent with our results of the strong positive relationship between the extreme precipitation and the monsoon indices.

In fact, the contributions from dynamics and thermodynamics to extreme precipitation have been studied extensively, with various conclusions drawn for different regions and conditions (e.g., Li et al., 2013; Seager et al., 2010; Yamada et al., 2021). A complete understanding of rainfall extremes should be achieved through state-of-the-art climate models, but this is hindered by substantial biases in current models (e.g., Seneviratne et al., 2021). The accurate simulation of rainfall extremes depends heavily on the ability of models to realistically capture the heavy rain-producing processes. Several factors can affect model performance in simulating these processes, such as model resolution (e.g., Sabin et al., 2013), representation of topography (e.g., Mishra et al., 2018), and convective parametrization (Bador et al., 2020). A recent study by You and Ting (2023), utilizing models from the CMIP6 High-Resolution Model Intercomparison Project (HighResMIP) for Asian rainfall extremes, found that high model resolution greatly enhances the simulation of rainfall extremes. Rainfall

10.1029/2024EA003563

Table 4
Regional Trends in Precipitation Indices for the Period 1971–2015

		APHRODITE			DHM		
	Index	Trend	Relative change (%)	Change per °C warming (%/°C)	Trend	Relative change (%)	Change per °C warming (%/°C)
HIR	RX1day	−0.10	−8.62	−7.44	−0.09	−7.48	−6.46
	RX5day	−0.14	−13.85	−11.95	−0.06	−13.26	−11.44
	R95pTOT	−1.80	−20.73	−17.89	−0.57	−20.64	−17.82
	R99pTOT	−0.84	−33.50	−28.91	−0.54	−22.95	−19.81
FR	R10 mm	−0.05	−10.85	−9.36	−0.06	−13.13	−11.33
	R20 mm	−0.04	−16.80	−14.50	−0.01	−11.95	−10.32
DR	CDD	0.16	2.59	2.24	0.43	19.58	16.90
	CWD	0.27	19.11	16.50	0.06	6.57	5.67
GN	PRCPTOT	−1.42	−10.19	−8.80	−1.17	−12.94	−11.17
	WD	0.02	−1.08	−0.93	−0.11	−7.03	−6.07
	SDII	−0.01	−7.09	−6.12	0.01	−5.67	−4.90

extremes are more pronounced on the windward side of steep topography, such as the foothills of the Himalayas, and in heavy monsoon regions such as central India, southern China, and the western North Pacific. These improvements are associated with a better representation of vertical ascents and the models' ability to simulate rain-producing synoptic low-pressure systems, which are more frequent and stronger at higher resolutions.

Apart from the aforementioned climatic factors, topography also plays a critical role in extreme precipitation changes in this mountainous country. Nepal's elevation rises sharply from about 300 m in the south to over 4,000 m in the north within a relatively short latitudinal span. Despite this, our spatial analysis of extreme precipitation revealed a west-east pattern, which does not align with the north-south elevation gradient. Additionally, we observed that data uncertainty increases with altitude. No observation stations are located above 3,000 m, leading to significant data gaps. In gridded data sets, substantial discrepancies exist among the four data sets we utilized, contributing to uncertainty in our conclusions (Figure S14 in Supporting Information S1). Comparisons between station data and gridded AHPRODITE data showed good correlation at lower altitudes but discrepancies at higher altitudes above 2,000 m in extreme precipitation events. Therefore, while topography was seriously considered, it did not play a critical role in our final results for Nepal. Apart from topography, we examined extreme precipitation across annual, monsoon season, and non-monsoon season periods and found similar patterns. To maintain a concise manuscript, we presented the most dominant results and omitted some detailed analyses.

Tropical and extra-tropical climate drivers such as the El Niño-Southern Oscillation (ENSO; Diaz and Markgraf (2000), Madden–Julian Oscillation (MJO; Madden and Julian (1971)), North Atlantic Oscillation (NAO; Branstator (2002)), Arctic Oscillation (AO; Thompson and Wallace (1998), Wallace (2000)) and the Indian Ocean Dipole mode (IOD; Saji et al. (1999)) also seems to impact significantly on extreme rain over Indian Subcontinent including Nepal (Barlow et al., 2005; Bhutiyani et al., 2010; Cannon et al., 2017; Rai et al., 2015; Roxy et al., 2019; Sabeerali et al., 2014). The reduction of monsoonal activity is found to be associated with a weakened connection between the El Niño/Southern Oscillation and the South Asian Summer Monsoon (Sano et al., 2013), and teleconnection patterns (Panagiotopoulos et al., 2002; Sheridan & Lee, 2012). Furthermore, the large-scale wave train over the North America–North Atlantic–Eurasia region could have important effects on the upper-level trend over the Himalayas (Wang et al., 2022). This wave train is a stationary pattern of atmospheric variability in the northern summer in the Eurasian mid-latitudes, resembling the circumglobal teleconnection (CGT) (Ding & Wang, 2005; Saeed et al., 2014).

3.3.4. Future Outlook

In our analysis, we observed that precipitation in Nepal exhibited an overall declining trend over the past 45 years, from 1971 to 2015, with a notable recovery occurring from 2003 to 2015. This temporal pattern highlights the complex nature of precipitation dynamics in Nepal, influenced by varying climatic conditions, time periods, and driving factors. Despite these fluctuations, the trend toward increasing precipitation and extreme precipitation events aligns with predictions of global warming. The latest projections from the ensemble averages of ESMs in the CMIP6 database indicate that Nepal's annual precipitation and extreme precipitation events are expected to continue rising until the end of the century under the SSP126, SSP245, and SSP585 scenarios (Almazroui et al., 2020; Seneviratne et al., 2021). These projections suggest that the overall increasing trend, despite periodic fluctuations, poses significant challenges for the country.

Yet, it is well worth bearing in mind that mechanisms of precipitation and extreme precipitation still remain unclear due to considerable uncertainty and spatial variations. The large uncertainty stems in part from the poor representation of atmospheric dynamics in ESM, which is related to the lack of recognition of the contribution of atmospheric dynamics to the control of historical precipitation, the lack of clarity in the description of physical processes at the convective scale, and the effect of rugged and complicated topography on the variability of moisture fluxes.

4. Conclusions

The analysis of extreme precipitation for a 45-year period in Nepal reveals a consistent drying trend, marked by significant decreases in high-intensity and frequency indices, along with notable increases in duration-related indices. Spatially, a heterogeneous pattern emerges, with a general declining trend but pockets of increase, particularly in the western part of Nepal. Overall, recent years show a distinctive spatial shift, notably a revival of extreme precipitation in the western regions, challenging the generally observed drying trend. The comparison between DHM and APHRODITE data sets highlights consistent trends, although APHRODITE data sets have larger bias to DHM over the regions above the 3,000 m elevation and the trends remained the same before and after bias correction. Amongst all the gridded data sets adopted by the study, APHRODITE performs the best.

The mechanisms driving extreme precipitation changes in Nepal are multifaceted, influenced by both large-scale and local atmospheric dynamics and a range of interconnected factors. On a larger scale, the South Asia Summer Monsoon, with correlations with extreme precipitation metrics highlights the pivotal role on extreme precipitation trends, especially the WYI index. Weakening monsoon circulation, influenced by factors like land-sea temperature contrast, contributes to the observed trends. Local-scale wind impacts and shifting atmospheric circulation patterns, notably around 2003, further explain spatial variations. The switch in precipitation patterns is largely ascribed to the shift of jet stream and its associated wind field changes. While thermodynamic contributions from increased moisture content due to warming play a role, the weakened monsoon circulation appears to counteract the anticipated increase in extreme precipitation. Future projections anticipate increased extreme precipitation, aligning with broader subcontinental trends.

Overall, the resurgence and escalating extreme precipitation, despite the prevailing drying climate regime over the past 45 years, pose unforeseen challenges to the local population and ecosystems in Nepal. These trends and shifts emphasize the multifaceted nature of climate variability and call for continued monitoring and analysis to understand and adapt to the changing precipitation dynamics in the region. The drying or wet trend of total precipitation has broader implications for water resources (i.e., foods in wet seasons and spring water supply in dry seasons), crop yields, and forest ecosystem management. Contemporary policies and adaptation strategies must consider the evolving complex climatic patterns and their multifaceted consequences in the region.

Data Availability Statement

The In-situ precipitation data used in this study were purchased from the Department of Hydrology and Meteorology of Nepal (DHM, 2022) with fee required. The precipitation gridded data sets were acquired from the Asian Precipitation–Highly-Resolved Observational Data Integration Towards Evaluation (APHRODITE, Yatagai et al., 2012); the Climate Hazards Group (CHIRPS, Funk et al., 2015); and the Third Pole High-resolution precipitation data set (TPHiPr, Jiang, Yi, et al., 2023). Other climate variables were obtained from the European Center for Medium-Range Weather Forecasts (ECMWF), data from ERA5 and ERA5-land data sets were used in the creation of this manuscript (Hersbach et al., 2023a, 2023b; Service, 2019). Three Monsoon indices were used, the WYI (Webster & Yang, 1992), the IMI (Parthasarathy et al., 1992), and the SASMI (Li & Zeng, 2002). Plotting and calculations are done in Jupyter version 2.1.5 in Python 3.0. Python software and documentation are licensed under PSF license (Sanner, 1999). Jupyter version 2.1.5 is licensed under the terms of the 3-Clause BSD

License (Granger & Pérez, 2021; JupyterLab, 2016). Figures were made with Matplotlib version 3.2.2 (Hunter, 2007; Matplotlib, 2020). The package RClimdex version 1.0 was used for analyzing extreme precipitation indices, and is under LGPL-2.1 license (Rclimdex, 2019; Zhang & Yang, 2004). R version 4.3.1 was used to run Rclimdex under GNU General Public License version 2 (Ihaka & Gentleman, 1996). In addition, QGIS 3.28.0-Firenze was used for mapping under GNU General Public License (Moyroud & Portet, 2018; Qgis, 2022).

Acknowledgments

This work was funded by the National Natural Science Foundation of China, International Joint Research Project "Developing Nature-based Solutions for Nepal Following a Nexus Approach towards Sustaining Forestry, Water Resources and Livelihoods" (Project ID: 42061144004). Partial support was from the Southern Research Station of the USDA Forest Service.

References

Aggarwal, D., Attada, R., Shukla, K., Chakraborty, R., & Kunchala, R. K. (2022). Monsoon precipitation characteristics and extreme precipitation events over Northwest India using Indian high resolution regional reanalysis. *Atmospheric Research*, *267*, 105993. https://doi.org/10.1016/j.atmosres.2021.105993

Allan, R. P., Willett, K. M., John, V. O., & Trent, T. (2022). Global changes in water vapor 1979–2020. *Journal of Geophysical Research: Atmospheres*, *127*(12), e2022JD036728. https://doi.org/10.1029/2022JD036728

Almazroui, M., Saeed, S., Saeed, F., Islam, M. N., & Ismail, M. (2020). Projections of precipitation and temperature over the South Asian countries in CMIP6. *Earth Systems and Environment*, *4*(2), 297–320. https://doi.org/10.1007/s41748-020-00157-7

Annamalai, H., Hafner, J., Sooraj, K., & Pillai, P. (2013). Global warming shifts the monsoon circulation, drying South Asia. *Journal of Climate*, *26*(9), 2701–2718. https://doi.org/10.1175/JCLI-D-12-00208.1

Aryal, A., Tran, T.-N.-D., Kumar, B., & Lakshmi, V. (2023). Evaluation of satellite-derived precipitation products for streamflow simulation of a mountainous Himalayan watershed: A study of Myagdi Khola in Kali Gandaki basin, Nepal. *Remote Sensing*, *15*(19), 4762. https://doi.org/10.3390/rs15194762

Bador, M., Boé, J., Terray, L., Alexander, L. V., Baker, A., Bellucci, A., et al. (2020). Impact of higher spatial atmospheric resolution on precipitation extremes over land in global climate models. *Journal of Geophysical Research: Atmospheres*, *125*(13), e2019JD032184. https://doi.org/10.1029/2019JD032184

Baidya, S. K., Shrestha, M. L., & Sheikh, M. M. (2008). Trends in daily climatic extremes of temperature and precipitation in Nepal. *Journal of Hydrology and Meteorology*, *5*(1), 38–51. Retrieved from https://soham.org.np/wp-content/uploads/2008/03/v5-38-51.pdf

Barlow, M., Wheeler, M., Lyon, B., & Cullen, H. (2005). Modulation of daily precipitation over southwest Asia by the Madden–Julian oscillation. *Monthly Weather Review*, *133*(12), 3579–3594. https://doi.org/10.1175/MWR3026.1

Bhutiyani, M. R., Kale, V. S., & Pawar, N. (2010). Climate change and the precipitation variations in the northwestern Himalaya: 1866–2006. *International Journal of Climatology: A Journal of the Royal Meteorological Society*, *30*(4), 535–548. https://doi.org/10.1002/joc.1920

Bohlinger, P., & Sorteberg, A. (2018). A comprehensive view on trends in extreme precipitation in Nepal and their spatial distribution. *International Journal of Climatology*, *38*(4), 1833–1845. https://doi.org/10.1002/joc.5299

Bollasina, M. A., Ming, Y., & Ramaswamy, V. (2011). Anthropogenic aerosols and the weakening of the South Asian summer monsoon. *Science*, *334*(6055), 502–505. https://doi.org/10.1126/science.1204994

Branstator, G. (2002). Circumglobal teleconnections, the jet stream waveguide, and the North Atlantic Oscillation. *Journal of Climate*, *15*(14), 1893–1910. https://doi.org/10.1175/1520-0442(2002)015<1893:CTTJSW>2.0.CO;2

Byrne, M. P., & O'Gorman, P. A. (2018). Trends in continental temperature and humidity directly linked to ocean warming. *Proceedings of the National Academy of Sciences*, *115*(19), 4863–4868. https://doi.org/10.1073/pnas.1722312115

Caesar, J., Alexander, L., Trewin, B., Tse-Ring, K., Sorany, L., Vuniyayawa, V., et al. (2011). Changes in temperature and precipitation extremes over the Indo-Pacific region from 1971 to 2005. *International Journal of Climatology*, *31*(6), 791–801. https://doi.org/10.1002/joc.2118

Cannon, F., Carvalho, L. M., Jones, C., Hoell, A., Norris, J., Kiladis, G. N., & Tahir, A. A. (2017). The influence of tropical forcing on extreme winter precipitation in the western Himalaya. *Climate Dynamics*, *48*(3–4), 1213–1232. https://doi.org/10.1007/s00382-016-3137-0

Dangol, S., Talchabhadel, R., & Pandey, V. P. (2022). Performance evaluation and bias correction of gridded precipitation products over Arun River Basin in Nepal for hydrological applications. *Theoretical and Applied Climatology*, *148*(3), 1353–1372. https://doi.org/10.1007/s00704-022-04001-y

DHM. (2022). Meteorological observations [Dataset]. *Department of Hydrology and Meteorology (DHM)*. https://www.dhm.gov.np/request-data

Diaz, H. F., & Markgraf, V. (2000). *El Niño and the southern Oscillation: Multiscale variability and global and regional impacts*. Cambridge University Press. https://doi.org/10.1017/cbo9780511573125.006

Ding, Q., & Wang, B. (2005). Circumglobal teleconnection in the northern hemisphere summer. *Journal of Climate*, *18*(17), 3483–3505. https://doi.org/10.1175/JCLI3473.1

Donat, M. G., Lowry, A. L., Alexander, L. V., O'Gorman, P. A., & Maher, N. (2016). More extreme precipitation in the world's dry and wet regions. *Nature Climate Change*, *6*(5), 508–513. https://doi.org/10.1038/nclimate2941

Duncan, J. M., Biggs, E. M., Dash, J., & Atkinson, P. M. (2013). Spatio-temporal trends in precipitation and their implications for water resources management in climate-sensitive Nepal. *Applied Geography*, *43*, 138–146. https://doi.org/10.1016/j.apgeog.2013.06.011

Easterling, D. R., Meehl, G. A., Parmesan, C., Changnon, S. A., Karl, T. R., & Mearns, L. O. (2000). Climate extremes: Observations, modeling, and impacts. *Science*, *289*(5487), 2068–2074. https://doi.org/10.1126/science.289.5487.2068

Fang, C., Haywood, J. M., Liang, J., Johnson, B. T., Chen, Y., & Zhu, B. (2023). Impacts of reducing scattering and absorbing aerosols on the temporal extent and intensity of South Asian summer monsoon and East Asian summer monsoon. *Atmospheric Chemistry and Physics*, *23*(14), 8341–8368. https://doi.org/10.5194/egusphere-2023-407

Fischer, E. M., & Knutti, R. (2015). Anthropogenic contribution to global occurrence of heavy-precipitation and high-temperature extremes. *Nature Climate Change*, *5*(6), 560–564. https://doi.org/10.1038/nclimate2617

Funk, C., Peterson, P., Landsfeld, M., Pedreros, D., Verdin, J., Shukla, S., et al. (2015). The climate hazards infrared precipitation with stations—A new environmental record for monitoring extremes. *Scientific Data*, *2*(1), 1–21. https://doi.org/10.1038/sdata.2015.66

Gao, J., He, Y., Masson-Delmotte, V., & Yao, T. (2018). ENSO effects on annual variations of summer precipitation stable isotopes in Lhasa, southern Tibetan Plateau. *Journal of Climate*, *31*(3), 1173–1182. https://doi.org/10.1175/JCLI-D-16-0868.1

Gao, S., Wang, L., Hao, L., & Sun, G. (2023). Community forestry dominates the recent land greening amid climate change in Nepal. *Environmental Research Letters*, *18*(10), 104014. https://doi.org/10.1088/1748-9326/acf8de

Ghosh, S., Vittal, H., Sharma, T., Karmakar, S., Kasiviswanathan, K. S., Dhanesh, Y., et al. (2016). Indian summer monsoon rainfall: Implications of contrasting trends in the spatial variability of means and extremes. *PLoS One*, *11*(7), e0158670. https://doi.org/10.1371/journal.pone.0158670

Goswami, B. N., Venugopal, V., Sengupta, D., Madhusoodanan, M., & Xavier, P. K. (2006). Increasing trend of extreme rain events over India in a warming environment. *Science*, *314*(5804), 1442–1445. https://doi.org/10.1126/science.1132027

Granger, B. E., & Pérez, F. (2021). Jupyter: Thinking and storytelling with code and data [Software]. *Computing in Science & Engineering*, *23*(2), 7–14. https://doi.org/10.1109/MCSE.2021.3059263

Guhathakurta, P., Sreejith, O., & Menon, P. (2011). Impact of climate change on extreme rainfall events and flood risk in India. *Journal of Earth System Science*, *120*(3), 359–373. https://doi.org/10.1007/s12040-011-0082-5

Gupta, V., Jain, M. K., Singh, P. K., & Singh, V. (2020). An assessment of global satellite-based precipitation datasets in capturing precipitation extremes: A comparison with observed precipitation dataset in India. *International Journal of Climatology*, *40*(8), 3667–3688. https://doi.org/10.1002/joc.6419

Hamed, K. H., & Rao, A. R. (1998). A modified Mann-Kendall trend test for autocorrelated data. *Journal of Hydrology*, *204*(1–4), 182–196. https://doi.org/10.1016/S0022-1694(97)00125-X

Hersbach, H., Bell, B., Berrisford, P., Biavati, G., Horányi, A., Muñoz Sabater, J., et al. (2023a). ERA5 hourly data on pressure levels from 1940 to present [Dataset]. *Copernicus Climate Change Service (C3S) Climate Data Store (CDS)*. https://doi.org/10.24381/cds.bd0915c6

Hersbach, H., Bell, B., Berrisford, P., Biavati, G., Horányi, A., Muñoz Sabater, J., et al. (2023b). ERA5 hourly data on single levels from 1940 to present [Dataset]. *Copernicus Climate Change Service (C3S) Climate Data Store (CDS)*. https://doi.org/10.24381/cds.adbb2d47

Hunter, J. D. (2007). Matplotlib: A 2D graphics environment [Software]. *Computing in Science & Engineering*, *9*(3), 90–95. https://doi.org/10.1109/mcse.2007.55

Ihaka, R., & Gentleman, R. (1996). R: A language for data analysis and graphics [Software]. *Journal of Computational & Graphical Statistics*, *5*(3), 299–314. https://doi.org/10.1080/10618600.1996.10474713

Jia, G., Shevliakova, E., Artaxo, P., de Noblet-Ducoudré, N., Houghton, R., House, J., et al. (2019). Land–climate interactions. In *Climate change and land: An IPCC special report on climate change, desertification, land degradation, sustainable land management, food security, and greenhouse gas fluxes in terrestrial ecosystems*. https://doi.org/10.1017/9781009157988.004

Jiang, H., Yi, Y., Xu, J., Chen, D., Lu, F., Li, R., et al. (2023). Characterizing precipitation uncertainties in a high-altitudinal permafrost watershed of the Tibetan plateau based on regional water balance and hydrological model simulations. *Journal of Hydrology: Regional Studies*, *47*, 101445. https://doi.org/10.1016/j.ejrh.2023.101445

Jiang, J., Zhou, T., Qian, Y., Li, C., Song, F., Li, H., et al. (2023). Precipitation regime changes in High Mountain Asia driven by cleaner air. *Nature*, *623*(7987), 1–6. https://doi.org/10.1038/s41586-023-06619-y

Jiang, Y., Yang, K., Qi, Y., Zhou, X., He, J., Lu, H., et al. (2023). TPHiPr: A long-term (1979–2020) high-accuracy precipitation dataset (1/30°, daily) for the Third Pole region based on high-resolution atmospheric modeling and dense observations [Dataset]. *Earth System Science Data*, *15*(2), 621–638. https://doi.org/10.5194/essd-15-621-2023

Jin, Q., & Wang, C. (2017). A revival of Indian summer monsoon rainfall since 2002. *Nature Climate Change*, *7*(8), 587–594. https://doi.org/10.1038/nclimate3348

JupyterLab. (2016). Jupyterlab [Software]. *GitHub repository*. https://github.com/jupyterlab/jupyterlab

Karki, R., Hasson, S. U., Schickhoff, U., Scholten, T., & Böhner, J. (2017). Rising precipitation extremes across Nepal. *Climate*, *5*(1), 4. https://doi.org/10.3390/cli5010004

Khatakho, R., Talchabhadel, R., & Thapa, B. R. (2021). Evaluation of different precipitation inputs on streamflow simulation in Himalayan River basin. *Journal of Hydrology*, *599*, 126390. https://doi.org/10.1016/j.jhydrol.2021.126390

Kotz, M., Levermann, A., & Wenz, L. (2022). The effect of rainfall changes on economic production. *Nature*, *601*(7892), 223–227. https://doi.org/10.1038/s41586-021-04283-8

Krishnan, R., Sabin, T., Vellore, R., Mujumdar, M., Sanjay, J., Goswami, B., et al. (2016). Deciphering the desiccation trend of the South Asian monsoon hydroclimate in a warming world. *Climate Dynamics*, *47*(3–4), 1007–1027. https://doi.org/10.1007/s00382-015-2886-5

Kulkarni, A. (2012). Weakening of Indian summer monsoon rainfall in warming environment. *Theoretical and Applied Climatology*, *109*(3–4), 447–459. https://doi.org/10.1007/s00704-012-0591-4

Kumar, M., Hodnebrog, Ø., Daloz, A. S., Sen, S., Badiger, S., & Krishnaswamy, J. (2021). Measuring precipitation in Eastern Himalaya: Ground validation of eleven satellite, model and gauge interpolated gridded products. *Journal of Hydrology*, *599*, 126252. https://doi.org/10.1016/j.jhydrol.2021.126252

Li, J., & Zeng, Q. (2002). A unified monsoon index [Dataset]. *Geophysical Research Letters*, *29*(8), 115-111–115-114. https://doi.org/10.1029/2001gl013874

Li, L., Li, W., & Barros, A. P. (2013). Atmospheric moisture budget and its regulation of the summer precipitation variability over the Southeastern United States. *Climate Dynamics*, *41*(3–4), 613–631. https://doi.org/10.1007/s00382-013-1697-9

Liu, B., Wu, G., Mao, J., & He, J. (2013). Genesis of the South Asian high and its impact on the Asian summer monsoon onset. *Journal of Climate*, *26*(9), 2976–2991. https://doi.org/10.1175/JCLI-D-12-00286.1

Lorenz, R., Argüeso, D., Donat, M. G., Pitman, A. J., van den Hurk, B., Berg, A., et al. (2016). Influence of land-atmosphere feedbacks on temperature and precipitation extremes in the GLACE-CMIP5 ensemble. *Journal of Geophysical Research: Atmospheres*, *121*(2), 607–623. https://doi.org/10.1002/2015jd024053

Luo, X., Fan, X., Li, Y., & Ji, X. (2020). Bias correction of a gauge-based gridded product to improve extreme precipitation analysis in the Yarlung Tsangpo–Brahmaputra River basin. *Natural Hazards and Earth System Sciences*, *20*(8), 2243–2254. https://doi.org/10.5194/nhess-20-2243-2020

Madden, R. A., & Julian, P. R. (1971). Detection of a 40–50 day oscillation in the zonal wind in the tropical Pacific. *Journal of the Atmospheric Sciences*, *28*(5), 702–708. https://doi.org/10.1175/1520-0469(1971)028<0702:DOADOI>2.0.CO;2

Maharjan, M., Yoneda, M., Talchabhadel, R., Thapa, B. R., & Aryal, A. (2023). Use of indices on daily timescales to study changes in extreme precipitation across Nepal over 40 Years (1976–2015). *Earth and Space Science*, *10*(1), e2020EA001509. https://doi.org/10.1029/2020EA001509

Mann, H. B. (1945). Nonparametric tests against trend. *Econometrica: Journal of the Econometric Society*, *13*(3), 245–259. https://doi.org/10.2307/1907187

Mason, R. B., & Anderson, C. E. (1963). The development and decay of the 100-mb. summertime anticyclone over southern Asia. *Monthly Weather Review*, *91*(1), 3–12. https://doi.org/10.1175/1520-0493(1963)091<0003:tdadot>2.3.co;2

Matplotlib. (2020). Matplotlib: Visualization with Python (version v3.2.2) [Software]. *The Matplotlib development team*. https://matplotlib.org/

Meehl, G. A., Shields, C. A., Arblaster, J. M., Neale, R., Hu, A., Annamalai, H., et al. (2023). Climate base state influences on South Asian monsoon processes derived from analyses of E3SMv2 and CESM2. *Geophysical Research Letters*, *50*(17), e2023GL104313. https://doi.org/10.1029/2023GL104313

Ménégoz, M., Gallée, H., & Jacobi, H. (2013). Precipitation and snow cover in the Himalaya: From reanalysis to regional climate simulations. *Hydrology and Earth System Sciences*, *17*(10), 3921–3936. https://doi.org/10.5194/hess-17-3921-2013

Mishra, S. K., Anand, A., Fasullo, J., & Bhagat, S. (2018). Importance of the resolution of surface topography in Indian monsoon simulation. *Journal of Climate*, *31*(12), 4879–4898. https://doi.org/10.1175/JCLI-D-17-0324.1

Mishra, V., Smoliak, B. V., Lettenmaier, D. P., & Wallace, J. M. (2012). A prominent pattern of year-to-year variability in Indian Summer Monsoon Rainfall. *Proceedings of the National Academy of Sciences*, *109*(19), 7213–7217. https://doi.org/10.1073/pnas.1119150109

Mohan, T., & Rajeevan, M. (2017). Past and future trends of hydroclimatic intensity over the Indian monsoon region. *Journal of Geophysical Research: Atmospheres*, *122*(2), 896–909. https://doi.org/10.1002/2016jd025301

Moyroud, N., & Portet, F. (2018). Introduction to QGIS [Software]. *QGIS and generic tools*, *1*, 1–17. https://doi.org/10.1002/9781119457091.ch1

Mukherjee, S., Aadhar, S., Stone, D., & Mishra, V. (2018). Increase in extreme precipitation events under anthropogenic warming in India. *Weather and Climate Extremes*, *20*, 45–53. https://doi.org/10.1016/j.wace.2018.03.005

Nie, J., Sobel, A. H., Shaevitz, D. A., & Wang, S. (2018). Dynamic amplification of extreme precipitation sensitivity. *Proceedings of the National Academy of Sciences*, *115*(38), 9467–9472. https://doi.org/10.1073/pnas.1800357115

Panagiotopoulos, F., Shahgedanova, M., & Stephenson, D. (2002). A review of Northern Hemisphere winter-time teleconnection patterns. *Journal de Physique IV*, *12*(10), 27–47. https://doi.org/10.1051/jp4:20020450

Pandey, V. P., Shrestha, D., & Adhikari, M. (2021). Characterizing natural drivers of water-induced disasters in a rain-fed watershed: Hydro-climatic extremes in the Extended East Rapti Watershed, Nepal. *Journal of Hydrology*, *598*, 126383. https://doi.org/10.1016/j.jhydrol.2021.126383

Panthi, J., Dahal, P., Shrestha, M. L., Aryal, S., Krakauer, N. Y., Pradhanang, S. M., et al. (2015). Spatial and temporal variability of rainfall in the Gandaki river basin of Nepal Himalaya. *Climate*, *3*(1), 210–226. https://doi.org/10.3390/cli3010210

Parthasarathy, B., Rupa Kumar, K., & Kothawale, D. (1992). Indian summer monsoon rainfall indices: 1871-1990 [Dataset]. *The Meteorological Magazine*, *121*(1441), 174–186. https://pascal-francis.inist.fr/vibad/index.php?action=getRecordDetail&idt=5436367

Pettitt, A. N. (1979). A non-parametric approach to the change-point problem. *Journal of the Royal Statistical Society: Series C (Applied Statistics)*, *28*(2), 126–135. https://doi.org/10.2307/2346729

Pfahl, S., O'Gorman, P. A., & Fischer, E. M. (2017). Understanding the regional pattern of projected future changes in extreme precipitation. *Nature Climate Change*, *7*(6), 423–427. https://doi.org/10.1038/nclimate3287

Pfahl, S., & Wernli, H. (2012). Quantifying the relevance of cyclones for precipitation extremes. *Journal of Climate*, *25*(19), 6770–6780. https://doi.org/10.1175/JCLI-D-11-00705.1

Pokharel, B., Wang, S. Y. S., Meyer, J., Marahatta, S., Nepal, B., Chikamoto, Y., & Gillies, R. (2020). The east–west division of changing precipitation in Nepal. *International Journal of Climatology*, *40*(7), 3348–3359. https://doi.org/10.1002/joc.6401

Qgis. (2022). QGIS - The leading open source desktop GIS (version v3.28 'Firenze') [Software]. *Open-Source Geospatial Foundation (OSGeo)*. https://qgis.org/en/site/forusers/download.html

Rai, A., Saha, S. K., Pokhrel, S., Sujith, K., & Halder, S. (2015). Influence of preonset land atmospheric conditions on the Indian summer monsoon rainfall variability. *Journal of Geophysical Research: Atmospheres*, *120*(10), 4551–4563. https://doi.org/10.1002/2015jd023159

Ramanathan, V., Chung, C., Kim, D., Bettge, T., Buja, L., Kiehl, J. T., et al. (2005). Atmospheric brown clouds: Impacts on South Asian climate and hydrological cycle. *Proceedings of the National Academy of Sciences*, *102*(15), 5326–5333. https://doi.org/10.1073/pnas.0500656102

Rclimdex. (2019). Simple R package for ETCCDI/CRD climate change indices calculations (Version v1.0) [Software]. *Github*. https://github.com/ECCC-CDAS/RclimDex

Roxy, M., Dasgupta, P., McPhaden, M. J., Suematsu, T., Zhang, C., & Kim, D. (2019). Twofold expansion of the Indo-Pacific warm pool warps the MJO life cycle. *Nature*, *575*(7784), 647–651. https://doi.org/10.1038/s41586-019-1764-4

Roxy, M. K., Ghosh, S., Pathak, A., Athulya, R., Mujumdar, M., Murtugudde, R., et al. (2017). A threefold rise in widespread extreme rain events over central India. *Nature Communications*, *8*(1), 1–11. https://doi.org/10.1038/s41467-017-00744-9

Roxy, M. K., Ritika, K., Terray, P., Murtugudde, R., Ashok, K., & Goswami, B. (2015). Drying of Indian subcontinent by rapid Indian Ocean warming and a weakening land-sea thermal gradient. *Nature Communications*, *6*(1), 7423. https://doi.org/10.1038/ncomms8423

Sabeerali, C., Rao, S. A., George, G., Rao, D. N., Mahapatra, S., Kulkarni, A., & Murtugudde, R. (2014). Modulation of monsoon intraseasonal oscillations in the recent warming period. *Journal of Geophysical Research: Atmospheres*, *119*(9), 5185–5203. https://doi.org/10.1002/2013jd021261

Sabin, T. P., Krishnan, R., Ghattas, J., Denvil, S., Dufresne, J.-L., Hourdin, F., & Pascal, T. (2013). High resolution simulation of the South Asian monsoon using a variable resolution global climate model. *Climate Dynamics*, *41*(1), 173–194. https://doi.org/10.1007/s00382-012-1658-8

Saeed, S., Van Lipzig, N., Müller, W. A., Saeed, F., & Zanchettin, D. (2014). Influence of the circumglobal wave-train on European summer precipitation. *Climate Dynamics*, *43*(1–2), 503–515. https://doi.org/10.1007/s00382-013-1871-0

Saha, A., Ghosh, S., Sahana, A., & Rao, E. (2014). Failure of CMIP5 climate models in simulating post-1950 decreasing trend of Indian monsoon. *Geophysical Research Letters*, *41*(20), 7323–7330. https://doi.org/10.1002/2014gl061573

Saha, U., & Sateesh, M. (2022). Rainfall extremes on the rise: Observations during 1951–2020 and bias-corrected CMIP6 projections for near-and late 21st century over Indian landmass. *Journal of Hydrology*, *608*, 127682. https://doi.org/10.1016/j.jhydrol.2022.127682

Saji, N., Goswami, B. N., Vinayachandran, P., & Yamagata, T. (1999). A dipole mode in the tropical Indian Ocean. *Nature*, *401*(6751), 360–363. https://doi.org/10.1038/43854

Sanner, M. F. (1999). Python: A programming language for software integration and development [Software]. *Journal of Molecular Graphics and Modelling*, *17*(1), 57–61. https://doi.org/10.1016/S1093-3263(99)99999-0

Sano, M., Tshering, P., Komori, J., Fujita, K., Xu, C., & Nakatsuka, T. (2013). May–September precipitation in the Bhutan Himalaya since 1743 as reconstructed from tree ring cellulose δ18O. *Journal of Geophysical Research: Atmospheres*, *118*(15), 8399–8410. https://doi.org/10.1002/jgrd.50664

Scussolini, P., Bakker, P., Guo, C., Stepanek, C., Zhang, Q., Braconnot, P., et al. (2019). Agreement between reconstructed and modeled boreal precipitation of the Last Interglacial. *Science Advances*, *5*(11), eaax7047. https://doi.org/10.1126/sciadv.aax7047

Seager, R., Naik, N., & Vecchi, G. A. (2010). Thermodynamic and dynamic mechanisms for large-scale changes in the hydrological cycle in response to global warming. *Journal of Climate*, *23*(17), 4651–4668. https://doi.org/10.1175/2010JCLI3655.1

Sen, P. K. (1968). Estimates of the regression coefficient based on Kendall's tau. *Journal of the American Statistical Association*, *63*(324), 1379–1389. https://doi.org/10.2307/2285891

Seneviratne, S. I., Wilhelm, M., Stanelle, T., van den Hurk, B., Hagemann, S., Berg, A., et al. (2013). Impact of soil moisture-climate feedbacks on CMIP5 projections: First results from the GLACE-CMIP5 experiment. *Geophysical Research Letters*, *40*(19), 5212–5217. https://doi.org/10.1002/grl.50956

Seneviratne, S. I., Zhang, X., Adnan, M., Badi, W., Dereczynski, C., Di Luca, A., et al. (2021). Weather and climate extreme events in a changing climate. In *Climate change 2021: The physical science basis. Contribution of working group I to the Sixth assessment report of the intergovernmental panel on climate change*. Cambridge University Press. https://doi.org/10.1017/9781009157896.013

Service, C. (2019). ERA5-Land hourly data from 1950 to present [Dataset]. *Copernicus Climate Change Service (C3S) Climate Data Store (CDS)*. https://doi.org/10.24381/CDS.E2161BAC

Sharma, S., Hamal, K., Khadka, N., & Joshi, B. B. (2020). Dominant pattern of year-to-year variability of summer precipitation in Nepal during 1987–2015. *Theoretical and Applied Climatology*, *142*(3), 1071–1084. https://doi.org/10.1007/s00704-020-03359-1

Shepherd, T. G. (2014). Atmospheric circulation as a source of uncertainty in climate change projections. *Nature Geoscience*, *7*(10), 703–708. https://doi.org/10.1038/ngeo2253

Sheridan, S., & Lee, C. C. (2012). Synoptic climatology and the analysis of atmospheric teleconnections. *Progress in Physical Geography*, *36*(4), 548–557. https://doi.org/10.1177/0309133312447935

Shrestha, A. B., Bajracharya, S. R., Sharma, A. R., Duo, C., & Kulkarni, A. (2017). Observed trends and changes in daily temperature and precipitation extremes over the Koshi river basin 1975–2010. *International Journal of Climatology*, *37*(2), 1066–1083. https://doi.org/10.1002/joc.4761

Shrestha, D., Sharma, S., Hamal, K., Jadoon, U. K., & Dawadi, B. (2021). Spatial distribution of extreme precipitation events and its trend in Nepal. *Environmental Sciences*, *9*(1), 58–66. https://doi.org/10.12691/aees-9-1-8

Shrestha, N. K., Qamer, F. M., Pedreros, D., Murthy, M., Wahid, S. M., & Shrestha, M. (2017). Evaluating the accuracy of Climate Hazard Group (CHG) satellite rainfall estimates for precipitation based drought monitoring in Koshi basin, Nepal. *Journal of Hydrology: Regional Studies*, *13*, 138–151. https://doi.org/10.1016/j.ejrh.2017.08.004

Shrestha, S., Yao, T., & Adhikari, T. R. (2019). Analysis of rainfall trends of two complex mountain river basins on the southern slopes of the Central Himalayas. *Atmospheric Research*, *215*, 99–115. https://doi.org/10.1016/j.atmosres.2018.08.027

Singh, D., Ghosh, S., Roxy, M. K., & McDermid, S. (2019). Indian summer monsoon: Extreme events, historical changes, and role of anthropogenic forcings. *Wiley Interdisciplinary Reviews: Climate Change*, *10*(2), e571. https://doi.org/10.1002/wcc.571

Singh, D., Tsiang, M., Rajaratnam, B., & Diffenbaugh, N. S. (2014). Observed changes in extreme wet and dry spells during the South Asian summer monsoon season. *Nature Climate Change*, *4*(6), 456–461. https://doi.org/10.1038/nclimate2208

Sun, G., Tiwari, K. R., Hao, L., Amatya, D., Liu, N., & Song, C. (2024). Climate change and forest hydrology in future forests. In *Future forests* (pp. 95–124). Elsevier. https://doi.org/10.1016/B978-0-323-90430-8.00003-4

Sun, J., & Ao, J. (2013). Changes in precipitation and extreme precipitation in a warming environment in China. *Chinese Science Bulletin*, *58*(12), 1395–1401. https://doi.org/10.1007/s11434-012-5542-z

Sun, Q., Zhang, X., Zwiers, F., Westra, S., & Alexander, L. V. (2021). A global, continental, and regional analysis of changes in extreme precipitation. *Journal of Climate*, *34*(1), 243–258. https://doi.org/10.1175/JCLI-D-19-0892.1

Tabari, H. (2020). Climate change impact on flood and extreme precipitation increases with water availability. *Scientific Reports*, *10*(1), 13768. https://doi.org/10.1038/s41598-020-70816-2

Talchabhadel, R., Aryal, A., Kawaike, K., Yamanoi, K., & Nakagawa, H. (2021). A comprehensive analysis of projected changes of extreme precipitation indices in West Rapti River basin, Nepal under changing climate. *International Journal of Climatology*, *41*(S1), E2581–E2599. https://doi.org/10.1002/joc.6866

Talchabhadel, R., Karki, R., Thapa, B. R., Maharjan, M., & Parajuli, B. (2018). Spatio-temporal variability of extreme precipitation in Nepal. *International Journal of Climatology*, *38*(11), 4296–4313. https://doi.org/10.1002/joc.5669

Thompson, D. W., & Wallace, J. M. (1998). The Arctic Oscillation signature in the wintertime geopotential height and temperature fields. *Geophysical Research Letters*, *25*(9), 1297–1300. https://doi.org/10.1029/98GL00950

Trenberth, K. E., Fasullo, J. T., & Shepherd, T. G. (2015). Attribution of climate extreme events. *Nature Climate Change*, *5*(8), 725–730. https://doi.org/10.1038/nclimate2657

Tuladhar, D., Dewan, A., Kuhn, M., & Corner, R. J. (2020). Spatio-temporal rainfall variability in the Himalayan mountain catchment of the Bagmati River in Nepal. *Theoretical and Applied Climatology*, *139*(1–2), 599–614. https://doi.org/10.1007/s00704-019-02985-8

Turner, A. G., & Annamalai, H. (2012). Climate change and the South Asian summer monsoon. *Nature Climate Change*, *2*(8), 587–595. https://doi.org/10.1038/nclimate1495

Upadhyay, S., Silwal, P., Prajapati, R., Talchabhadel, R., Shrestha, S., Duwal, S., & Lakhe, H. (2022). Evaluating magnitude agreement and occurrence consistency of CHIRPS product with ground-based observations over medium-sized river basins in Nepal. *Hydrology*, *9*(8), 146. https://doi.org/10.3390/hydrology9080146

Vellore, R. K., Kaplan, M. L., Krishnan, R., Lewis, J. M., Sabade, S., Deshpande, N., et al. (2016). Monsoon-extratropical circulation interactions in Himalayan extreme rainfall. *Climate Dynamics*, *46*(11–12), 3517–3546. https://doi.org/10.1007/s00382-015-2784-x

Vellore, R. K., Krishnan, R., Pendharkar, J., Choudhury, A. D., & Sabin, T. (2014). On the anomalous precipitation enhancement over the Himalayan foothills during monsoon breaks. *Climate Dynamics*, *43*(7–8), 2009–2031. https://doi.org/10.1007/s00382-013-2024-1

Vinnarasi, R., & Dhanya, C. (2016). Changing characteristics of extreme wet and dry spells of Indian monsoon rainfall. *Journal of Geophysical Research: Atmospheres*, *121*(5), 2146–2160. https://doi.org/10.1002/2015jd024310

Wallace, J. M. (2000). North Atlantic oscillatiodannular mode: Two paradigms—One phenomenon. *Quarterly Journal of the Royal Meteorological Society*, *126*(564), 791–805. https://doi.org/10.1002/qj.49712656402

Wang, B., & Ding, Q. (2006). Changes in global monsoon precipitation over the past 56 years. *Geophysical Research Letters*, *33*(6). https://doi.org/10.1029/2005gl025347

Wang, B., & Fan, Z. (1999). Choice of South Asian summer monsoon indices. *Bulletin of the American Meteorological Society*, *80*(4), 629–638. https://doi.org/10.1175/1520-0477(1999)080<0629:COSASM>2.0.CO;2

Wang, Z., Duan, A., Yang, S., & Ullah, K. (2017). Atmospheric moisture budget and its regulation on the variability of summer precipitation over the Tibetan Plateau. *Journal of Geophysical Research: Atmospheres*, *122*(2), 614–630. https://doi.org/10.1002/2016jd025515

Wang, Z., Lin, L., Zhang, X., Zhang, H., Liu, L., & Xu, Y. (2017). Scenario dependence of future changes in climate extremes under 1.5 C and 2 C global warming. *Scientific Reports*, *7*(1), 46432. https://doi.org/10.1038/srep46432

Wang, Z., Yang, S., Luo, H., & Li, J. (2022). Drying tendency over the southern slope of the Tibetan Plateau in recent decades: Role of a CGT-like atmospheric change. *Climate Dynamics*, *59*(9–10), 2801–2813. https://doi.org/10.1007/s00382-022-06262-9

Webster, P. J., & Yang, S. (1992). Monsoon and ENSO: Selectively interactive systems [Dataset]. *Quarterly Journal of the Royal Meteorological Society*, *118*(507), 877–926. https://doi.org/10.1002/qj.49711850705

Wei, W., Zou, S., Duan, W., Chen, Y., Li, S., Sayama, T., & Zhu, J. (2024). Increased population exposures to extreme precipitation in Central Asia under 1.5°C and 2°C global warming scenarios. *Geography and Sustainability*, *5*(3), 343–356. https://doi.org/10.1016/j.geosus.2024.02.005

Yamada, T. J., Hoshino, T., & Suzuki, A. (2021). Using a massive high-resolution ensemble climate data set to examine dynamic and thermodynamic aspects of heavy precipitation change. *Atmospheric Science Letters*, *22*(12), e1065. https://doi.org/10.1002/asl.1065

Yao, T., Thompson, L., Chen, D., Zhang, Y., Wang, N., Zhao, L., et al. (2020). Third Pole climate warming and cryosphere system changes. *World Meteorological Organization Bulletin*, *69*(1), 38–44. Retrieved from https://public.wmo.int/en/resources/bulletin/third-pole-climate-warming-and-cryosphere-system-changes

Yao, T., Thompson, L., Yang, W., Yu, W., Gao, Y., Guo, X., et al. (2012). Different glacier status with atmospheric circulations in Tibetan Plateau and surroundings. *Nature Climate Change*, *2*(9), 663–667. https://doi.org/10.1038/nclimate1580

Yatagai, A., Kamiguchi, K., Arakawa, O., Hamada, A., Yasutomi, N., & Kitoh, A. (2012). Aphrodite: Constructing a long-term daily gridded precipitation dataset for Asia based on a dense network of rain gauges [Dataset]. *Bulletin of the American Meteorological Society*, *93*(9), 1401–1415. https://doi.org/10.1175/BAMS-D-11-00122.1

Yigez, B., Xiong, D., Belete, M., Zhang, B., Azene, B., Baig, M. A., et al. (2022). Evaluation of multi-satellite precipitation products for soil loss and sediment export modeling over eastern regions of the Koshi River Basin, Nepal. *Journal of Soils and Sediments*, *22*(10), 2731–2749. https://doi.org/10.1007/s11368-022-03264-2

You, Y., & Ting, M. (2023). Improved performance of high-resolution climate models in simulating Asian monsoon rainfall extremes. *Geophysical Research Letters*, *50*(5), e2022GL100827. https://doi.org/10.1029/2022GL100827

Yue, S., & Wang, C. Y. (2002). Applicability of prewhitening to eliminate the influence of serial correlation on the Mann-Kendall test. *Water Resources Research*, *38*(6), 4-1–4-7. https://doi.org/10.1029/2001WR000861

Zhang, X., Alexander, L., Hegerl, G. C., Jones, P., Tank, A. K., Peterson, T. C., et al. (2011). Indices for monitoring changes in extremes based on daily temperature and precipitation data. *Wiley Interdisciplinary Reviews: Climate Change*, *2*(6), 851–870. https://doi.org/10.1002/wcc.147

Zhang, X., & Yang, F. (2004). RClimDex (1.0) user manual [Software]. *Climate Research Branch Environment Canada*, *22*, 13–14. https://www.acmad.net/rcc/procedure/RClimDexUserManual.pdf